

AD-A200 145

DTIC FILE COPY
UNCLASSIFIED

2

SECURITY CLASSIFICATION OF THIS PAGE (When Data Entered)

REPORT DOCUMENTATION PAGE		READ INSTRUCTIONS BEFORE COMPLETING FORM
1. REPORT NUMBER TR- 88-1018	2. GOVT ACCESSION NO.	3. RECIPIENT'S CATALOG NUMBER
4. TITLE (and Subtitle) Nonlinear Dynamic Response of Composite Rotor Blades		5. TYPE OF REPORT & PERIOD COVERED Final Report 1 Dec 1985 - June 1988
6. AUTHOR(s) John J. Engblom, Ozden O. Ochoa		7. PERFORMING ORG. REPORT NUMBER ME 5375-8
8. PERFORMING ORGANIZATION NAME AND ADDRESS Texas A&M University Mechanical Engineering Department College Station, TX 77843		9. CONTRACT OR GRANT NUMBER(s) F49620-86-K-0003
10. CONTROLLING OFFICE NAME AND ADDRESS Air Force Office of Scientific Research/NA Building 410 Bolling AFB, DC 20332		11. PROGRAM ELEMENT, PROJECT, TASK AREA & WORK UNIT NUMBERS 61102f, 2302, B1
12. MONITORING AGENCY NAME & ADDRESS (if different from Controlling Office) Same as 11		13. REPORT DATE August 1988
		14. NUMBER OF PAGES 44 plus Appendices
		15. SECURITY CLASS. (of this report) Unclassified
		16. DECLASSIFICATION, DOWNGRADING SCHEDULE
17. DISTRIBUTION STATEMENT (of this Report) Approved for Public Release, Distribution Unlimited		
18. DISTRIBUTION STATEMENT (of the abstract entered in Block 20, if different from Report) DTIC ELECTE S OCT 06 1988 D		
19. SUPPLEMENTARY NOTES		
20. KEY WORDS (Continue on reverse side if necessary and identify by block number) Composite Materials, Interlaminar Shear and Normal Stresses, Nonlinear Dynamic Response, Assumed Displacement and Hybrid Models, Damage Mechanisms, Finite Elements, Large Displacement Formulation (JES)		
21. ABSTRACT (Continue on reverse side if necessary and identify by block number) Summarized are research activities related to Nonlinear Dynamic Response of Composite Rotor Blades. Fundamental to the analysis is the development of a continuum formulation that can accurately account for the effects of interlaminar shear and interlaminar normal stress variation thru-the-thickness of a laminate. Technical highlights of the research efforts to date are presented for each of the proposed tasks; namely, Nonlinear Displacement Formulation for Composite Media, Incorporate Damage Mechanisms into Dynamic Response Formulation and Correlation of Formulated Response Model with Experimental data.		

DD FORM 1 JAN 73 1473

EDITION OF 1 NOV 65 IS OBSOLETE

UNCLASSIFIED

SECURITY CLASSIFICATION OF THIS PAGE (When Data Entered)

88 10 5 297

TABLE OF CONTENTS

	Page
I. Overview and Summary	1
II. Summary by Task	6
II.1. Task I: Nonlinear Displacement Formulation for Composite Media	6
II.1.1 Continuum Formulation	6
II.1.2 Large-Displacement Formulation	10
II.1.3 Computer Implementation	13
II.1.4 Analytical Verification	17
II.2. Task II: Incorporate Damage Mechanisms into Dynamic Response Formulation	23
II.3. Task III: Correlation of Formulated Response Model with Experimental Data	35
III. References	36
IV. Related Activities	39
V. Tables and Figures	43



Accession For	
NTIS CRA&I	<input checked="checked" type="checkbox"/>
DTIC TAB	<input type="checkbox"/>
Unannounced	<input type="checkbox"/>
Justification	
By	
Distribution/	
Availability Codes	
DAI	Avail and/or Special
A-1	

1. OVERVIEW AND SUMMARY

Fundamental to this work has been the development of a continuum formulation that can accurately account for the effects of interlaminar shear and interlaminar normal stress variation through-the-thickness of a laminate. Furthermore, emphasis has been particularly on tapered-twisted airfoil geometries which can be analytically represented as an assemblage of thin to moderately thick finite elements. To achieve solution efficiencies, various plate/shell type elements have been developed in this work as opposed to the more computationally intensive solid type elements.

On the basis of these requirements, alternative continuum formulations have been considered and are herein denoted as the (i) Higher Order Displacement, (ii) Modified-Kirchhoff and (iii) Hybrid Stress formulations, respectively. "Shear deformable" elements, based on the former two formulations, have been incorporated in a computer code and tested on the basis of correlations with known analytical, numerical, and experimental solutions. Numerous tests have been performed for static, dynamic and buckling behavior of laminated structures. Both plate and "doubly-curved" shell elements have been formulated and successfully tested. Note that use of a shell element is an especially efficient approach in modelling airfoil geometries.

Significant efforts have also been devoted to developing a suitable large displacement formulation. Due to the requirement

that interlaminar stresses be accurately represented, a total Lagrangian formulation has been utilized and based upon the complete Green's strain tensor. A geometric and large-displacement stiffness formulation, based upon a form of the nonlinear strain-nodal displacement relationship, has been developed and numerically implemented for one of the developed "shear deformable" plate elements.

Since emphasis in this work focused on the development of incremental response solutions, including damage effects, the computational approach needed to have the capability to (i) predict and differentiate between relevant failure modes, (ii) modify constitutive equations appropriately and (iii) perform equilibrium iterations to assure stress redistribution based upon the extent of damage. Use of "piecewise smooth" failure criteria based on various types of damage has provided a good basis for incrementally tracking damage. This approach has been incorporated in the computer code using various stress criteria. Alternative strain-based and energy-based approaches have been considered including the representation of damage via the use of internal state variables.

Note that integration for an element is performed on a layer-by-layer basis which allows for damage effects to be characterized at the layer level. Herein a layer refers to either a lamina or to a subset of adjacent laminae having equal ply orientations. It is noteworthy that variation in strain energy

can be calculated as damage accumulates and that such information can provide the basis for evaluating sub-laminate buckling and even delamination growth.

Experimental data has been utilized to substantiate both stiffness reduction and damage predictions. The data is in the form of failure strengths for laminates and material moduli variations.

Computational efficiencies have been achieved in the numerical procedures primarily by using an equilibrium formulation to obtain the transverse stresses. This approach minimizes the need for 3-D solid elements. Furthermore, a "reduced basis" approach for computing nonlinear dynamic response has been developed and partially implemented in the computer code.

In summary, the utility of the developed "shear deformable" elements, and in particular the use of an equilibrium formulation to obtain the transverse stresses, has been demonstrated for laminated composite geometries. Realistic structures can be modelled with the use of a mesh generator, which has been developed in order to generate airfoil geometries. Since solutions for airfoil response were not available with which to validate the computer formulation, laminated composite cylinders, with various boundary conditions, were modelled to demonstrate the capability of the formulation to determine transverse stresses in "curved" geometries. These stresses are essential in the

determination of damage accumulation because of the typically low interlaminar strength exhibited by laminated composite materials.

Excellent damage predictions have been obtained by coupling the formulation with piecewise continuous stress criteria which provide the basis for differentiating between damage modes. These modes include fiber fracture, and tensile-compressive matrix cracking, including arrays of both intralaminar and interlaminar cracks. Strain energy calculations have been performed to determine the variation in strain energy release rate along the boundary of an interior debonded region. These calculations are based on the assumption of a relatively thin sublaminar bounded by a rigid "parent".

The numerical formulation developed in this work is especially suited to analyzing the nonlinear effects and damage progression in actual structures., e.g., the response of an airfoil to foreign object damage or the response of a helically wound cylinder to a tool drop. It is noted that "scaled down" analyses have been performed for primarily two reasons: (1) the lack of data with which to correlate the results and (2) the solutions to date have been obtained on a mini-computer, while timely solutions for the examples cited would have to be obtained on a mainframe. With regard to the second point, it would be worthwhile to either "vectorize" the computer formulation or to convert the code to a parallel processing format.

The sublaminar analysis could be made more realistic by considering boundary conditions that reflect the actual displacement/slope conditions at the delamination front. This approach is achievable through more computational effort, focused on accounting for the generalized forces/displacement that occur along the boundary of the debonded region. These boundary conditions could be supplied by the complete (global) finite element model to a local model of the delaminated region.

Finally, there are strain-based and energy-based damage criteria that have the potential for providing more accurate damage predictions than those obtained herein using stress criteria. Implementing such criteria in the numerical model, however, would require significant experimental effort to determine certain phenomenological constants needed to relate constitutive behavior to damage progression.

II. SUMMARY BY TASK

This section presents technical highlights of the research efforts to date for each of the three tasks. Details of the analytical formulation are presented in the Appendices.

II.1. TASK I: Nonlinear Displacement Formulation for Composite Media

II.1.1 Continuum Formulation

Two variational principles, the principle of minimum potential energy and the principle of modified complementary energy, are generally used to develop two distinctly different finite element models, the assumed displacement model and the hybrid stress model respectively. These models incorporate the effects of transverse shear and normal deformations whose contributions are recognized as essential for accurate laminate analysis [1-10]. In the present work, emphasis has been placed on developing displacement based models.

Within the displacement formulation, element stiffness matrices are determined for each element, these matrices are then assembled to represent the final system of equations and a solution procedure for the unknown nodal displacements is provided. Coordinate transformations to describe ply orientations of a composite media are taken into account. The in-plane stresses are calculated from constitutive relations of orthotropic

continuum whereas transverse shear and normal stresses are calculated from equilibrium considerations. Finite element models have been tested for static, dynamic and buckling behavior. The test problems and the results are presented in Section II.1.4. The finite element models are herein briefly discussed.

A. Higher Order Displacement Formulation

The through-the-thickness effects can be incorporated into the analysis by choosing a displacement field that eliminates two major shortcomings of the classical plate theory; namely normals remain normal and in-plane displacements are linear through the thickness. These shortcomings are eliminated by prescribing independently the reference surface displacements and rotations of the normal and including higher order terms for in-plane displacements. This is accomplished in the plate element formulation by the following variation

$$u(x,y,z) = u_0(x,y) + z\psi_x(x,y) + z^2\phi_x(x,y)$$

$$v(x,y,z) = v_0(x,y) + z\psi_y(x,y) + z^2\phi_y(x,y)$$

$$w(x,y,z) = w_0(x,y)$$

The neutral surface displacements are represented by u_0, v_0 and w_0 , the rotation about the y-axis is denoted by ψ_x and the rotation about the x-axis is ψ_y . The coefficients of z^2 , i.e., ϕ_x and ϕ_y , are contributions from transverse deformations [5,6] and have been found to be significant for unsymmetric laminate geometries.

These terms can be omitted in the analysis of symmetric laminates by imposing the appropriate constraints.

In the shell formulation, the displacement field is more complex in that it includes components of the surface unit-normal vector and three rotational components. The displacement components become

$$u(x,y,z) = u_0(x,y) + z[N_z\psi_x(x,y) - N_y\psi_z(x,y)]$$

$$v(x,y,z) = v_0(x,y) + z[N_z\psi_y(x,y) + N_x\psi_z(x,y)]$$

$$w(x,y,z) = w_0(x,y) - z[N_x\psi_x(x,y) + N_y\psi_y(x,y)]$$

where N_x , N_y and N_z are components of the surface normal at a particular (x,y,z) coordinate location for the element. The shell displacements degenerate to those of a plate for $N_z = 1$ and $N_x = N_y = 0$ as expected. Note that z^2 terms are not included in the displacement field for the shell element.

The elements developed are designated as the quadrilateral higher order displacement (QHD) models. QHD40 is an eight-noded plate element with seven degrees of freedom (three midsurface displacements, two rotations and two higher order terms for in-plane displacements) per corner node and three degrees of freedom (transverse midsurface displacement and two rotations) per mid-state node. QHD48 and QHD48S are eight-noded plate and shell elements respectively, with six degrees of freedom (three midsurface displacements and three rotations) per node. Element

QHD28 is a simplified version of QHD40, for which the mid-side nodes are eliminated. It should be noted that when the two higher order terms for in-plane displacements at each corner node are omitted, QHD28 reduces to the widely used four-noded bilinear plate element (QHD20). These elements produce either a quadratic or cubic variation in the transverse shear stress.

B. Modified-Kirchhoff Formulation

The Kirchhoff-Love assumption for normals to the reference surface is relaxed by incorporating shear rotations as additional degrees of freedom in the formulation [10]. Thus the assumed displacement field allows the transverse shear deformations but neglects the transverse normal deformations. The rotations γ_x and γ_y are incorporated in the displacement variation for the plate as follows

$$\begin{aligned} w(x,y) &= w_0(x,y) \\ u(x,y,z) &= u_0(x,y) - z \left(\frac{\partial w}{\partial x} + \gamma_x \right) \\ v(x,y,z) &= v_0(x,y) - z \left(\frac{\partial w}{\partial y} + \gamma_y \right) \end{aligned}$$

The transverse displacement $w(x,y)$ is chosen such that it will produce stress fields that characterize the transverse effects accurately.

This approach has been implemented in the formulation of an

eight-node quadrilateral plate element with 32 degrees of freedom-QD32, and various triangular elements. The stress fields obtained for these elements represent a quadratic transverse shear stress variation. The quadrilateral element produced the best results using this formulation.

II.1.2 Large Displacement Formulation

Inclusion of geometrically nonlinear effects in the formulation must be based upon the geometry to be analyzed and upon the type of stress prediction capabilities desired. The classical approach to thin plate analysis has been to use the Kirchhoff-Love assumptions in conjunction with the nonlinear von Karman relations [11,12]. As previously indicated, the Kirchhoff-Love assumptions are relaxed in this work to allow for a more accurate definition of interlaminar stress variation. These stresses can vary substantially through-the-thickness for the geometries of interest, i.e., thin to moderately thick plate type structures. The complete Green's strain tensor is utilized in this work, therefore, to account for all significant contributions to the interlaminar stress field. With respect to fixed Cartesian coordinates, x , y , and z , the strain tensor has the form

$$\epsilon_x = \frac{\partial u}{\partial x} + \frac{1}{2} \left[\left(\frac{\partial u}{\partial x} \right)^2 + \left(\frac{\partial v}{\partial x} \right)^2 + \left(\frac{\partial w}{\partial x} \right)^2 \right]$$

$$\gamma_{xy} = \frac{\partial u}{\partial y} + \frac{\partial v}{\partial x} + \left[\frac{\partial u}{\partial x} \frac{\partial u}{\partial y} + \frac{\partial v}{\partial x} \frac{\partial v}{\partial y} + \frac{\partial w}{\partial x} \frac{\partial w}{\partial y} \right]$$

where u , v and w represent displacements in the x, y, z coordinate directions, respectively. Note that the other strain components are obtained by a suitable permutation. In small-displacement analysis, the quadratic terms are neglected to give simply the linear strain approximation.

Based on the Green's strain tensor, the strain to nodal point displacement relationship can be specified for elements under development. It takes the form

$$\{\epsilon\} = [B]\{\Delta\}$$

Where $\{\epsilon\}$ is the vector of strain components, $\{\Delta\}$ the vector of nodal point displacements and $[B]$ a function of derivatives of the element shape functions. The quadratic terms in the strain tensor result in $[B]$ being a function of displacement state and, therefore, an incremental equilibrium formulation is required. The incremental strain-nodal displacement relationship takes the form

$$\{\delta\epsilon\} = ([B_0] + [B_L]) \{\delta\Delta\}$$

where $\{\delta\epsilon\}$ and $\{\delta\Delta\}$ represent incremental strains and nodal displacements, respectively, $[B_0]$ and $[B_L]$ are the small and large displacement contributions to the incremental strains. Based on the incremental equilibrium equations, the displacement formulation gives the force-displacement relationships

$$[K_0] = \int_V [B_0]^T [D] [B_0] dv$$

$$[K_L] = \int_V \left([B_0]^T [D] [B_L] + [B_L]^T [D] [B_L] + [B_L]^T [D] [B_0] \right) dv$$

where $[D]$ is an elasticity matrix obtained simply from the constitutive equations and integration is over the volume V of the element. $[K_0]$ is denoted the small-displacement stiffness matrix and $[K_L]$ is denoted the large-displacement stiffness matrix. Since response is also a function of stress state, the geometrical stiffness matrix $[K_G]$ is required and is obtained from

$$[K_G]\{\delta\Delta\} = \int_V \delta[B_L]^T \{\sigma\} dv$$

where $\{\sigma\}$ is the vector of stress components.

Inertial effects are analytically treated as a mass matrix $[M]$ which is a function of density and the element shape functions. These matrix forms are required in formulating static/dynamic response solutions and the incremental equilibrium equations have the general form

$$[M]\{\delta u\} + ([K_0] + [K_L] + [K_G]) \{\delta u\} = \{\delta F\}$$

where the mass and stiffness matrices represent an assembly of the elemental matrices previously discussed, $\{\delta u\}$ and $\{\delta u\}$ represent

the incremental displacements and accelerations for the mathematical model and $\{\delta F\}$ represents the vector of incrementally applied forces.

A complete geometrically nonlinear formulation, for static and dynamic response calculations, has been implemented in the computer code only for the QHD48 element. Linear elastic buckling analysis has been performed, however, with each of the elements, i.e., with $[K_L]$ omitted from the equation above.

II.1.3 Computer Implementation

Computer coding has been developed for the purpose of implementing the various continuum formulations. The code has served to generate static, dynamic and buckling solutions using different element formulations. All of the element integration is performed on a layer-by-layer basis through-the-thickness of the laminate. This approach is fundamental to the inclusion of damage mechanisms in the formulation.

Since solution of the equilibrium equations is a vital component in the overall solution strategy, it is appropriate to discuss the numerical methodology used in solving these equations. The intent is to obtain a higher ordered variation of the transverse shear and normal stresses (σ_{xz} , σ_{yz} , and σ_{zz}) than can be obtained via the constitutive equations. The solution procedure can be thought of as described below. Assume that the

in-plane stresses (σ_{xx} , σ_{yy} , σ_{xy}) within each layer of a particular element have been determined at selected locations, i.e., through solution of the constitutive equations. In the code as presently written, these locations are specified as the element centroid and element nodal points. The equilibrium equations (in the absence of body forces) have the indicial form

$$\sigma_{ij,j} = 0$$

from which it follows that the through-the-thickness shear stress variation can be written in numerical form for the i^{th} layer as

$$\Delta\sigma_{xz_i} = -(\sigma_{xx,x} + \sigma_{xy,y})_i \Delta Z_i$$

and

$$\Delta\sigma_{yz_i} = -(\sigma_{xy,x} + \sigma_{yy,y})_i \Delta Z_i.$$

Here, the left-hand-side represents the change in stress from the lower to the upper surface of the i^{th} layer and ΔZ_i is the thickness of the i^{th} layer at a particular location. The derivatives with respect to x and y in the expressions above are readily computed; this is because in-plane stresses within a layer are related to element displacements through derivatives of element shape functions, in conjunction with a material definition.

For an n layered laminate, n equations can be written in terms of both the unknown shear stresses at layer interfaces and the shear stresses at the laminate surfaces. Assuming the laminate has shear-free surfaces, the equations above give n equations in $n-1$ unknowns, so that, the equation set is over-determined. The equations have the matrix form below

$$\begin{matrix}
 \begin{bmatrix} 1 & & & \\ -1 & 1 & & \\ & -1 & 1 & \\ & & & 1 \\ & & & & -1 \end{bmatrix} & \begin{Bmatrix} \sigma_{xz_2} \\ \vdots \\ \sigma_{xz_n} \end{Bmatrix} & = & \begin{Bmatrix} I_{xz_1} \\ \vdots \\ I_{xz_n} \end{Bmatrix} \\
 n \times (n-1) & (n-1) \times 1 & & (n \times 1)
 \end{matrix}$$

where $I_{xzi} = -(\sigma_{xx,x} + \sigma_{xy,y})_i \Delta z_i$ and σ_{xzj} represents the shear stress acting at the interface of the $j-1^{\text{th}}$ and j^{th} layer. A similar equation set is obtained by replacing σ_{xzj} with σ_{yzj} and I_{xzi} with I_{yzi} . These equations are solved by utilizing a least-squares orthonormalization procedure [13]. Due to the simplicity of the terms in the coefficient matrix, a concise closed-form solution is obtained. Having determined the transverse shear stresses, the transverse normal stress variation is determined through the numerical form of the third equilibrium equation of the i^{th} layer

$$\Delta \sigma_{zz_i} = -(\sigma_{xz,x} + \sigma_{yz,y})_i \Delta z_i$$

As before, the left-hand-side represents the change in stress

through the i^{th} layer. Appropriate polynomial functions are utilized to describe the σ_{xz} and σ_{yz} in-plane variation. These functions are differentiated to obtain the right-hand-side of the equations above. Again the equation set is overdetermined because the normal tractions are known at the laminate surfaces. Solving for σ_{zz} proceeds, therefore, in identically the same manner as discussed in calculating σ_{xz} and σ_{yz} . Parenthetically, inclusion of body forces can be accomplished with little difficulty.

As a final note with regard to solving the equilibrium equations, note that the stresses coming from the constitutive equations are computed in an "element" coordinate system. In the special case of a shell element, these coordinates are generally not directed in either tangent-to or normal-to the shell directions. An additional computational requirement in this case is, therefore, to transform the "constitutive" stresses from element to shell coordinates. This allows numerical integration to proceed on a layer-by-layer basis in a direction normal to the shell surface, and assures that the stresses are determined with accuracy.

Successful application of the Higher Order Displacement type elements for particularly thin geometries requires the use of reduced numerical integration. This approximation technique brings along the choice of implementing it overall or selectively to the strain energy components. For the QHD plate formulations, only the transverse shear components are integrated with reduced

order [14-16]. Good results are obtained with the shell formulations by under-integrating all strain energy terms.

A reduced basis numerical algorithm has been developed and studied with respect to predicting the response of geometrically nonlinear systems. Good results have been obtained for some classical problems. The computational efficiency of this approach, however, is only realized when applied to a very large ordered system of equations.

A preprocessor has been developed to generate the finite element mesh for an airfoil shape of multiple-circular-arc geometry. Nodal coordinates, element connectivity and unit surface normals are all generated on the basis of limited geometrical input for a number of spanwise locations on a blade. The normal vector definitions are needed in implementing the QHD48S shell element. Typical mesh geometries are shown in Figures 1 and 2. The preprocessor can also generate finite element meshes for the special case of a cylindrical shape, which has proven very useful in some of the verification testing presented in the next section.

II.1.4. Analytical Verification

Significant verification results relating to the developed plate and shell element performance have been presented in previous technical reports submitted under Contract No.

F49620-82-K-0032. Much of these efforts are also reported in the papers and presentations listed in Section V (Related Activities) of this report. Static, dynamic (fundamental frequency and transient) and buckling response predictions for various laminate geometries are included in these results and will not be repeated herein. It is noteworthy that the QHD formulation gives the best results overall and that the elements are suitable for the study of damage accumulation in laminated composite structures.

Results comparing the performance of the QHD48 plate and QHD48S shell elements have not previously been presented. Each of these elements has six degrees of freedom per node and is similar, in this regard, to other elements found in the literature. The formulation is unique, however, due to the layer-by-layer approach to obtaining the transverse stresses through use of the equilibrium equations. This is the common thread linking all of the elements developed in this work. For the QHD48 plate element, 3 x 3 Gaussian quadrature along with 2x2 quadrature for the transverse shear components is employed. The element exhibits six rigid body modes and does not yield any undesirable spurious modes. In the shell formulation, 2x2 Gaussian quadrature is used to integrate all strain energy terms. This numerical approach produces six rigid body modes plus an additional zero-energy mode. This additional mode has not been shown to have a deleterious effect upon element performance.

QHD48 and QHD40 element formulations produce essentially

identical results for cylindrically bent and rectangular flat plates. In addition, the QHD48 element has been used to model both helically wound and cross-ply composite cylinders. First considered is a long cylinder under an internal pressure of 50 PSI, with inner diameter 36 in., thickness of 0.36 in. and cylinder length of 53 in. The laminate geometry is given as $[35.3^\circ, -35.3^\circ, 35.3^\circ, -35.3^\circ, 35.3^\circ]_s$. The orthotropic lamina properties are defined as

$$E_L = 5.136 \times 10^6 \text{ PSI}$$

$$E_T = 1.522 \times 10^6 \text{ PSI}$$

$$G_{LT} = 0.439 \times 10^6 \text{ PSI}$$

$$\nu_{LT} = 0.281$$

and typical results are given in Figures 3 and 4. It is interesting to note that the deformation is not axisymmetric as might be assumed. Results compare quite favorably with those obtained using a 3-D solid finite element formulation [17].

The QHD48 plate and QHD48S shell element formulations have been utilized to calculate the transverse shear stress variation that occurs in the 'boundary layer' region of a laminated cylindrical shell. Some of the results are compared to those given in [18], which presented an analytical solution specifically for determining the interlaminar stresses in laminated cylindrical shells. Plate/shell solutions are compared to those given in [18] for a three-layer, cross-ply wound cylinder. Fiber orientation is

defined as $[0^\circ, 90^\circ, 0^\circ]$ and results are obtained for two different sets of boundary conditions including both simply-supported and clamped ends. The cylinder geometry and loading is the same for all results presented herein. The cylinder has a length $L = 50$ inches, radius $R = 25$ inches and wall thickness $t = 0.25$ inches. Also, the cylinder is subjected to a uniform internal pressure of 100 psi. Two material systems are considered as defined below

Boron-Epoxy:

$$E_L = 32.5 \text{ MPsi}$$

$$E_T = 1.84 \text{ MPsi}$$

$$G_{LT} = 0.642 \text{ MPsi}$$

$$\nu_{LT} = 0.256$$

Glass-Epoxy:

$$E_L = 6.00 \text{ MPsi}$$

$$E_T = 1.50 \text{ MPsi}$$

$$G_{LT} = 0.80 \text{ MPsi}$$

$$\nu_{LT} = 0.25 \text{ MPsi}$$

The assumed material properties and geometry definitions are all consistent with those given in [18].

Since the laminated geometry under consideration is symmetric, only one quadrant of the cylinder with suitably specified boundary conditions need be modelled. Two levels of mesh refinement have been used to assure that convergent solutions

have been obtained. These include both 10x10 and 16x16 rectangular meshes. These meshes along with the geometry are shown in Figure 5. Note that all of the solutions presented herein are for the more refined mesh. Calculated values for the longitudinal transverse shear stress, τ_{yz} , occurring at the interface of the 0° and 90° layers are given in Figures 6-9. The first two of these Figures relate to the Boron-Epoxy material system, while the latter two Figures provide results for the Glass-Epoxy system. Regardless of which boundary condition is considered, the results indicate essentially zero transverse stresses away from the end constraint. Whereas in the vicinity of the cylinder end, a 'boundary layer' develops in which the transverse stresses become quite significant. As demonstrated in these Figures, the calculated transverse stresses are in excellent agreement with the analytical solutions given by Waltz [18]. Note that the shell element model gives better agreement with the analytical solution than does the plate element model, as would be expected. While the 10x10 mesh results are not presented herein for these cases, the solutions compare well with the 16x16 results and do demonstrate convergence.

Finally, calculated transverse stresses are presented for a cylindrical shell with a quasi-isotropic layup having ply sequence $[0^\circ, +45^\circ, -45^\circ, 90^\circ]_s$. The material system is assumed to be the Glass-Epoxy previously defined, while the geometry and loading are unchanged. Figures 10 and 11 present the transverse stress ' τ_{yz} ' variation calculated using the plate and shell element

formulations, again for both clamped and simply-supported boundary conditions. The 'boundary layer' stresses are similar to those shown in the previous cases. Based on the previous examples, it is believed that the shell element provides the more accurate results. All stress results represent average values at selected node points on the model. It is interesting to note that the variation in these stresses, i.e., at a particular node shared by more than one element, is much less pronounced in the shell than in the plate formulation. It seems this is simply a further indication that the shell formulation is more suitable in modelling structures having curvature.

Some verification testing of a developed "reduced basis" algorithm has also been performed for some classical problems. These include the large displacement transient response of both cantilevered and clamped-clamped beams subjected to step loading. Results are given in Figures 12 and 13 demonstrating the accuracy obtained in these problems compared to directly integrating all of the dynamical equations. Note that the basis vectors are comprised of both Ritz vectors and derivatives of Ritz vectors. The efficiencies obtained in using these vectors to obtain solutions for linear dynamical systems has been shown in [19, 20]. Reducing the order of the equations can be effective when the equations do not need to be updated very often during the course of a transient response analysis. Furthermore, the utility in such an approach is only realized in studying the response of large-ordered systems of equations.

II.2. TASK II: Incorporate Damage Mechanisms into Dynamic Response Formulation

Relevant failure modes of interest include those listed below

- (i) fiber fracture
- (ii) fiber-matrix debonding
- (iii) matrix cracking (parallel and transverse to fibers)
- (iv) delamination
- (v) buckling (possibly at layer or sub-laminate level)

Several smooth failure criteria, e.g., [21-24] have been developed in recent years to represent the failure of composites. These criteria, to varying degrees, can predict "failure" but do not identify a particular mode of failure. In performing incremental "damage" analysis, it is essential to both predict failure and to characterize it, e.g., do fibers rupture, does delamination occur, etc. The computational approach must, therefore, differentiate between viable failure modes and appropriately alter the constitutive equations on an incremental basis.

Stress Based Approach

One approach is to implement a piecewise smooth failure criteria, e.g., [25] in the finite element formulation. The general failure criteria is then comprised of m separate inequalities of the form

$$F_j(\{\sigma\}) < 1 ; j = 1, 2, \dots, m$$

at the layer level within each element. These criteria should differentiate between (i) tensile and compressive fiber failure, (ii) tensile and compressive matrix failure and (iii) delamination at layer interfaces due to either maximum stress or buckling considerations.

As progressive damage occurs throughout incremental loading (whether it be static or dynamic), it is essential that violation of failure criteria inequalities be reflected in modification of the material properties. This can be achieved by modifying the appropriate terms in the constitutive equations to reflect "stiffness reduction". When the strain varies between tension and compression, as in the case of transient dynamic response, the numerical model must reflect the differences in moduli related to whether or not an array of cracks is predicted to be opened or closed.

In conjunction with the above it is essential to perform equilibrium iterations within each analysis increment. This is required to assure that stress redistribution is properly accounted for as damage progresses.

The piecewise smooth failure criteria currently implemented in the incremental analysis are primarily due to Hashin [25], Lee [26], Greszczuk [27] and Hahn [28]. Layer stresses are defined as shown in Figure 14 and the criteria are summarized as follows:

Fiber Failure

1. Tension

The simplest criterion for tensile failure of a composite is the maximum stress criteria. The failure occurs if the fiber tensile stress exceeds the allowable normal strength σ_{FN}

$$\sigma_L \geq \sigma_{FN}$$

However, this is a drastic approximation, since the fibers vary significantly in their strength. Lee proposes that in addition to checking this criterion, the fibers fail if

$$(\sigma_{LT}^2 + \sigma_{LZ}^2)^{1/2} \geq \sigma_{FS}$$

where σ_{FS} is the fiber shear strength. On the other hand, the criterion proposed by Hashin for the tensile fiber failure is

$$\left(\frac{\sigma_L}{\sigma_{FN}} \right)^2 + \frac{1}{\sigma_{FS}^2} \left(\sigma_{LT}^2 + \sigma_{LZ}^2 \right) = 1$$

2. Compression

For compressive loads applied along the fiber direction, a proposed failure mechanism is analogous to the buckling of a column. The critical fiber buckling stress in the shear mode is given by Greszczuk and Hahn as

$$\sigma_{CS} = \frac{G_r}{(1-k)}$$

where G_r is the resin modulus, and k is the volume fraction ratio.

Matrix Failure

1. Tension

The composite tensile strength transverse to the fibers is not expected to deviate significantly from the matrix tensile strength. The tensile criteria used are as follows

$$\text{Lee } \sigma_T \geq \sigma_{MN} \quad \text{or } (\sigma_{TL}^2 + \sigma_{TZ}^2)^{1/2} \geq \sigma_{MS}$$

$$\text{Hashin } \frac{1}{\sigma_{MN}^2} (\sigma_T + \sigma_Z)^2 + \frac{1}{\sigma_{MS}^2} (\sigma_{TZ}^2 - \sigma_T \sigma_Z) + \frac{1}{\sigma_{FS}^2} (\sigma_{LT}^2 + \sigma_{LZ}^2) = 1$$

where $(\sigma_T + \sigma_Z) > 0$

The matrix normal strength and the matrix shear strength are denoted as σ_{MN} and σ_{MS} , respectively.

2. Compression

Under compression, failure may occur by shearing along a surface through the matrix parallel to the fiber axis. The criterion that describes this is proposed by Hashin.

$$\frac{1}{\sigma_{MNC}^2} \left[\left(\frac{\sigma_{MNC}}{2\sigma_{MS}} \right)^2 - 1 \right] (\sigma_T + \sigma_Z) + \frac{1}{4\sigma_{MS}^2} (\sigma_T + \sigma_Z)^2 + \frac{1}{\sigma_{MS}^2} (\sigma_{TZ}^2 - \sigma_T \sigma_Z) + \frac{1}{\sigma_{FS}^2} (\sigma_{LT}^2 + \sigma_{LZ}^2) = 1$$

where σ_{MNC} is the compressive matrix strength.

Delamination

Lee proposes that delamination occurs if either

$$\sigma_z \geq \sigma_{DN} \quad \text{or} \quad (\sigma_{LZ}^2 + \sigma_{TZ}^2)^{1/2} \geq \sigma_{DS}$$

where σ_{DN} and σ_{DS} are the through-the-thickness tensile and shear strengths respectively. Yet another form used by the authors to identify delamination is as follows

$$\left(\frac{\sigma_z}{\sigma_{DN}} \right)^2 + \frac{\sigma_{LT}^2 + \sigma_{TZ}^2}{\sigma_{DS}^2} \geq 1$$

Sublaminar Buckling

High interlaminar stresses that cause delaminations in composite components often cause localized buckling subsequent to delamination. These high stresses may promote the growth of the buckled delaminated region and lead to structural failure [29]. This instability related crack growth can be studied by the virtual crack closure technique as proposed by Whitcomb [30]. Simply, one identifies the delamination zone and addresses the layers above the delamination line as a "sublaminar" region and the layers below as a "parent" region. In this initial model, parent is assumed to be rigid. Therefore, one models only the sublaminar region as a plate with clamped boundaries. Figure 15 describes the geometry of the model. The reactions that are

calculated at the boundaries serve as forces that are used to close the debonded region (crack). The total strain energy release rate is calculated from the following expression,

$$G = 0.5 * (N_x \epsilon_x + N_y \epsilon_y + N_{xy} \epsilon_{xy} + M_x K_x + M_y K_y + M_{xy} K_{xy}).$$

Then, the distribution in the strain energy release rate is calculated as a function of the debond geometry.

Damage Prediction Calculations (Stress Based Approach)

The damage histories for selected composite laminates subjected to both in-plane and bending loads have been determined. Note that both static and transient dynamic loading conditions have been considered.

Uniaxial Tension: Response to Static Load

The one element plate model of Figure 16 is employed for the uniaxial tension analysis of angle-ply laminates. The laminate consists of three layers of T300/5208 graphite epoxy. Two stacking sequences are studied; namely, $[\theta^\circ/0^\circ/-\theta^\circ]_s$ and $[\theta^\circ/90^\circ/-\theta^\circ]_s$. The material and the strength properties of T300/5208 are given in Table 1. The first and last ply failure curves of the two laminates as a function of Theta are shown in Figures 17 and 18 for a statically applied load. As expected, the first and the last ply failures for uniaxial laminates of

$[\theta^\circ/0^\circ/\theta^\circ]_s$ of Figure 17 occur simultaneously, except for angles greater than 30° , they are quite separated. The $[\theta^\circ/90^\circ/\theta^\circ]_s$ layup of figure 18 shows that for $\theta=60^\circ$, 75° , and 90° laminates, the initial and final failures coincide, whereas for angles less than 60° , they are easily distinguished. Table 2 displays an alternate view of the damage progression in a $[15^\circ, 90^\circ, -15^\circ]_s$ laminate, where initial failure occurred at the 60th load increment and the final failure at the 117th increment. The column headings of Table 2; TF, CF, TM, CM and DL denote Tensile Fiber Failure, Compressive Fiber Failure, Tensile Matrix Failure, Compressive Matrix Failure, and Delamination, respectively. Note that the first ply failure was matrix failure in the 90° plys followed by the fiber failure in the angle plys. Thus one can easily identify the failure mode within a ply for a given load increment.

Uniaxial Tension: Critically Damped Response to Step Load

The same uniaxial tension model described above is used by the incremental dynamic analysis. To verify the dynamic response routines, all modes in the transient response are critically damped to approximate an incremental static solution. The first and last ply failures are predicted for the same stacking sequences as described in the incremental static analysis. The results for the $[\theta^\circ/0^\circ/\theta^\circ]_s$ stacking sequence are shown in Figure 19. The first and last ply failures occur simultaneously for $\theta=0^\circ$, 15° and 30° . These results compare quite well with the

Tsai-Wu failure criteria and those obtained in the incremental static analysis. Likewise, the predicted first and last ply failures for the stacking sequence $[0^\circ/90^\circ/-\theta^\circ]_s$ compared exceptionally well with the Tsai-Wu failure criteria and with data obtained from the incremental static analysis (Figure 20). Table 3 displays the progression of damage within the $[15^\circ/90^\circ/-15^\circ]_s$ laminate. The first ply failure occurred in the matrix of the 90° plies at the 50th load-time increment. The final failure occurred in the fibers of the 15° plies at the 97th load-time increment. The damage progression predicted by the incremental dynamic analysis is, therefore, quite similar to that obtained using the incremental static analysis.

Uniaxial Bar: Transient Response to Rectangular Pulse

A $[60^\circ/0^\circ/-60^\circ]_s$ T300/5208 graphite/epoxy bar is analyzed for the effects of damage on the transient response. The bar has a length to height ratio of 16. Damping is not included in this particular analysis. The composite bar is loaded with a rectangular pulse load equivalent to 45 percent of the last ply static failure load for the laminate. The duration of the pulse is 1.5 times the fundamental period of the bar. The $[60^\circ/0^\circ/-60^\circ]_s$ composite bar is analyzed both with no residual compressive stiffness and with ninety percent residual stiffness after a tensile failure mode has occurred. The transient response of the damaged laminate compared to the linear dynamic response is presented in Figure 21. In the figure, the tip displacement is

normalized by the maximum amplitude obtained by the linear dynamic solution and time is normalized by the fundamental period of the bar. At point A, matrix cracks develop in the 60° plies in elements 1-7. at point B, the maximum tip displacement is greater in the damaged laminate with no residual compressive stiffness than in the damaged laminate with ninety percent residual compressive stiffness.

Due to the development of tensile matrix damage, the amplitude is increased in the first cycle. The time period for the damaged transient response also tends to increase as damage lowers the stiffness properties of the laminate. The damaged laminate with no residual compressive stiffness exhibits a higher compressive tip displacement than either the linear dynamic solution or the damaged laminate with ninety percent residual compressive stiffness. This is caused by the lower compressive stiffness of the damaged laminate.

These results demonstrate that even for very simple geometries, it is essential that the effective material moduli, due to the opening/closing of crack arrays, be realistically characterized in the numerical modelling process.

Four-Point Bending: Response to Static Load

The bending problem of Figure 22 is modelled with four elements. The material and strength properties are as listed in

Table 1. The laminate is unidirectional and consists of twenty-four layers. For the bending problem, as discussed by Whitney [31], the critical aspect ratio is defined as $S = \sigma_{\max} / \tau_{\max}$, and for the present geometry, it is 22. Delamination is observed for aspect ratios less than the critical in the middle of the laminate as the load is increased. Additional matrix and fiber failure accompany delamination as shown in Table 4. The interaction curve of Figure 23 reveals that the final failure occurs after twenty percent load increase over the initial failure load. It should be noted that for aspect ratios less than the critical, the percent increase of the initial failure load to that of final failure load is constant; thus if one reduces the shear strength by the same percentage, the final failure load of the corresponding aspect ratio ends up on the interaction curve. This phenomenon is illustrated by the dash-lines of Figure 11. When the aspect ratios are higher than the critical, i.e., thin plate, the fiber failure at the outermost laminae proceeds rapidly toward the center and within four percent increase of the initial load, ultimate laminate failure occurs. A typical damage progression is displayed in Table 4 for an aspect ratio of 100. It is also of interest to observe the growth of failure as a function of the total strain energy. Figure 24 presents the variation of total strain energy in each lamina of a $[0^\circ]_{24}$ laminate with an aspect ratio of sixteen. As can be observed, as the load is increased, the strain energy increases in a layer until that layer undergoes failure, in which case the strain energy is lower than its previous value. This is depicted in layers 12 - 20, where failure

is observed; however, the undamaged layers 1 - 11 and 21 - 24 still maintain higher strain energy values as load is increased. Figure 25 focuses on the same information as Figure 24, yet provides a close-up of the energy variation in layers 5 through 20. As discussed above; as failure is detected, the strain energy in a layer decreases and causes the discontinuity in the quadratic curve. Note that the failure is observed as starting from the middle layers. On the other hand, for an aspect ratio of 100, as shown in Figure 26, the failure starts from the outermost laminae. In this case, the damaged layers are 1 - 4 and 20 - 24.

Strain Energy Release Rate Calculations

A quarter of a square, debonded sublaminar region is modelled as shown in Figure 27. A transverse point load is applied at the center. The strain energy release rate is calculated from

$$G = 0.5 \cdot D_{11} (M/P)^2$$

where D_{11} is the bending stiffness, M and P are the reaction moment and applied transverse load, respectively.

Simple examples are chosen to evaluate the strain energy release rate along the edge of the debond, for isotropic and orthotropic layups, namely; $[0^\circ]_4$, $[90^\circ]_4$, $[45^\circ - 45^\circ]_S$. Figure 28 illustrates the distribution of G along the y -axis for the layups considered. The magnitude of the total strain energy is the area under the respective curves for each case. For all cases, it is

observed that the delamination will grow at the midsides where G is highest.

Strain Based Approach

An alternative to modifying the constitutive equations based on violation of stress failure criteria, is to use a strain based approach that represents the accumulation of damage through definition of internal state variables in conjunction with experimentally determined phenomenological constants. The internal state variables can be represented as vectors having direction (orientation of damage) and magnitude (extent of damage). This approach should give good accuracy in characterizing the type of damage that develops first, i.e., intraply matrix cracking. This approach, combined with the stress criteria for fiber failure and delamination, should provide more accurate predictions than provided by use of the stress criteria alone. To be consistent with the finite element formulations developed in this work, it is important that damage be characterized at the layer level. A laminate damage model, in combination with experimental results for certain balanced laminates, can serve to define the needed layer damage model. These models, along with results for moduli variation as a function of damage accumulation, have been presented and discussed in the previous report under this project. While these models have been formulated, they have not been implemented in the computer formulation. It is emphasized that a significant amount of experimentation, probably using non-standard

test specimens, would be needed to fully implement such an approach to modelling damage accumulation.

II.3.3 TASK III: Correlation of Formulated Response Model with Experimental Data

Failure results presented in the previous section do compare well with the experimental data given in [32]. Additional experimental results, while not plentiful, do exist for cases in which data has been generated to quantify the effects of damage for various loading conditions. For example, the extent of damage is quantified in [33,34] for the impact response of composite plates. Correlation of the present formulation with such additional data would be a worthwhile endeavor.

III. REFERENCES

1. Whitney, J.M., "The Effects of Transverse Shear Deformation on the Bending of Laminated Plates," J. Composite Materials, 1969, Vol. 3, p. 534.
2. Pagano, N.J., "Stress Fields in Composite Laminates," Int. J. Solids and Structures, 1978, Vol. 14, p. 385-400.
3. Barker, R.M., Fu-Tien Lin, Dana, J.R., "Three Dimensional Finite Element Analysis of Laminated Composites," Computers & Structures, 1972 Vol. 2, p. 1013-1029.
4. Pian, T.H.H., and Tong, P., "Finite Element Methods in Continuum Mechanics," Advances in Applied Mechanics, 1972, Vol. 2, p. 1-58.
5. Reddy, J.N., "Bending of Laminated Anisotropic Shells by a Shear Deformable Finite Element," Fiber Science and Technology, 1982, Vol. 2, p. 9-24.
6. Pagano, N.J., "On the Calculation of Interlaminar Normal Stress in Composite Laminates," J. of Composite Materials, 1974, Vol. 8, p. 65-81.
7. Spilker, R.L., Chow, S.C. and Orringer, O., "Alternate Hybrid-Stress Elements for Analysis of Multilayer Composite Plates," J. Composite Materials, 1977, Vol. 11, p. 51-70.
8. Mau, S.T., Tong, P., and Pian, T.H.H., "Finite Element Solutions for Laminated Thick Plates," J. Composite Materials, 1972, Vol. 6, p. 304-305.
9. Pagano, N.J., "Exact Solutions for Composite Laminates in Cylindrical Bending," J. Composite Materials, 1969, Vol. 3, p. 398-411.
10. Pryor, C.W., and Barker, R.M., "Finite Element Analysis Including Transverse Shear Effects for Application to Laminated Plates," AIAA Journal, 1971, p. 912-917.
11. Whitney, J.M., and Leissa, A.W., "Analysis of Heterogeneous Anisotropic Plates," Journal of Applied Mechanics, 1969, Vol 36, p. 261-266.
12. Giri, J., and Simites, G.K., "Deflection Response of General Laminated Composite Plates to In-Plane and Transverse Loads," Fiber Science and Technology, 1980, Vol. 13, p. 225-242.
13. Whittaker, E. and Robinson, G., The Calculus of Observations, Blackie and son, Limited, Glasgow, 1944.

14. O.C. Zienkiewicz, R.L. Taylor and J.M. Too, 'Reduced Integration Technique in General Analysis of Plates & Shells', Int. J. Num. Meth. Engrg. 3, 275-290 (1971).
15. E.D.L. Pugh, E. Hinton, and O.C. Zienkiewicz, 'A Study of Quadrilateral Plate Bending Elements with Reduced Integration' Int. J. Num. Meth. Engrg. 12, 1059-1079 (1978).
16. T.J.R. Hughes, M. Cohen and M. Haroun, 'Reduced and Selective Integration Techniques in the Finite Element Analysis of Plates', Nucl. Eng. Des. 46, 203-222 (1978).
17. R. Natarajan, S.V. Hoa and T. S. Sankar, "Stress Analysis of Filament Wound Tanks Using Three-Dimensional Finite Elements", Int. J. Num. Meth. Engrg., 23, 623-633, 1986.
18. Waltz, T. L. and J. R. Vinson, "Interlaminar Stresses in Laminated Cylindrical Shells of Composite Materials," AIAA Journal, Vol. 14, No. 9, p. 1213-1218, Sept. 1976.
19. Wilson, E.L., Yuan, M.W., and Dickens, J.M., "Dynamic Analysis by Direct Superposition of Ritz Vectors," Earthquake Engineering and Structural Dynamics, Vol. 10, 813-821, 1982.
20. Kline, K.A., "Dynamic Analysis Using a Reduced Basis of Exact Modes and Ritz Vectors," AIAA Journal, Vol. 24, No. 12, 1986.
21. Hill, R., "A Theory of the Yielding and Plastic Flow of Anisotropic Materials," Proceedings of the Royal Society, London, 1948, Series A, Vol. 193, p. 281-290.
22. Tsai, S.W., "Strength Characteristics of Composite Materials," NASA CR-224, 1965.
23. Hoffman, I., "The Brittle Strength of Orthotropic Materials," J. Composite Materials, 1967, Vol. 1, p. 200-206.
24. Tsai, S.W. and Wu, E.M., "A General Theory of Strength for Anisotropic Materials," J. Composite Materials, 1971, Vol. 5, p. 58-81.
25. Hashin, Z., "Failure Criteria for Unidirectional Fiber Composites," J. Applied Mechanics, Vol. 47, 1980, p. 329.
26. Lee, J.D., "Three Dimensional Finite Element Analysis of Damage Accumulation in Composite Laminate," Computers & Structures, Vol. 15, No. 3, 1982, p. 335.
27. Greszczuk, L.B., "Microbuckling of Lamina-Reinforced Composites," Composite Materials: Testing and Design(third conference), ASTM STP 546, American Society for Testing and Materials, 1974, p.5.

28. Hahn, H.T. and Williams, J.G., "Compression Failure Mechanisms in Unidirectional Composites," Unpublished.
29. Ochoa, O.O. and Moore, A.J., "A Parametric Study on Strain Energy Release Rates of Compression Members," International Journal of Composite Structures, Accepted for Publication, 1988.
30. Whitcomb, J.D. and Shivakumar, R.N., "Strain Energy Release Rate Analysis of a Laminate with Postbuckled Delamination, NASA Technical Memorandum 89091, February, 1987.
31. Whitney, J.M. and Browning, C.W., "On Interlaminar Beam Experiments for Composite Materials," Proceedings of the 5th International Congress on Experimental Mechanics, June 10-15, 1984, Montreal.
32. Soni, S.R., "A New Look at Commonly Used Failure Theories in Composite Laminates," 24th Structures, Structural Dynamics and Materials Conference, A Collection of Technical Papers, AIAA/ASME/ASCE/AHS, Lake Tahoe, 1983, p.171.
33. Daniel, I.M. and Wooh, S.C., "Deformation and Damage of Composite Plates Under Impact Loading," Proceedings of International Symposium on Composite Materials and Structures, pp. 630-637, June 1986.
34. Ramkumar, R.L. and Thakar, Y.R., "Dynamic Response of Curved Laminated Plates Subjected to Low Velocity Impact," J. of Engineering Materials and Technology, Vol. 109, pp. 67-71, January 1987.

IV. RELATED ACTIVITIES

Technical Publications:

Havelka, J. J. and Engblom, J. J., "An Analysis of the Progression of Damage in Laminated Composites Under Transient Loading," Proceedings of the Pan American Congress of Applied Mechanics, Rio de Janeiro, Brazil, January 3 - 6, 1989.

Fuehne, J. P. and Engblom J. J., "A Doubly Curved, Shell Finite Element Formulation Including Transverse Shear Effects for Composite Shell Structures," Transactions of the 4th Japan-U.S. Conference on Composite Materials," Washington, D.C., June 27-29, 1988.

Hamdallah, J. M. and Engblom J. J., "Finite Element Plate Formulation Including Transverse Shear Effects for Representing Composite Shell Structures," Accepted for Publication in Journal of Reinforced Plastics and Composites.

Ochoa, O.O. and Moore, A.J., "A Parametric Study on Strain Energy Release Rates of Compression Members", International Journal of Composite Structures, 1988 [accepted for publication].

Fuehne, J. P. and Engblom J. J., "A Shear Deformable, Doubly-Curved Finite Element for the Analysis of Laminated Composite Structures," Accepted for Publication in Composite Structures.

Engblom, J. J., "Modelling the Effects of Intraply Cracking in Composite Laminates at the Sublaminar Level," Proceedings of the ASME Pressure Vessels and Piping Conference, San Diego, CA, June 29-July 2, 1987.

Hamdallah, J. M. and Engblom, J. J., "Finite Element Plate Formulation Including Transverse Shear Effects for Representing Composite Shell Structures," Proceedings of Joint Symposium on Composite Materials Science and Engineering, University of Delaware, September 23-25, 1987.

Ochoa, O. O. and Engblom, J. J., "Analysis of Progressive Failure in Composites," Composites Science and Technology, Vol. 28, pp. 87-102, 1987.

Kozma, F.K. and Ochoa, O.O., "Buckling of Composite Plates Using Shear Deformable Elements," AIAA Journal, Vol. 24, pp. 1721, 1986.

Engblom, J. J., Fox, N. P. and Ochoa, O. O., "Transient Response of Cross-and-Angle-Plyed Composite Plates Due to Transverse Loading," Proceedings of International Conference on Computational Mechanics, May 25-29, 1986, Ch. 4, pp. 191-196, Tokyo, Japan.

Ochoa, O. O., Kozma, F. and Engblom, J. J., "Stability Analysis of Composite Plates," Proceedings of International Conference on Computational Mechanics, May 25-29, 1986, Ch. 4, pp. 161-166, Tokyo, Japan.

Ochoa, O. O. and Engblom, J. J., "Analysis of Progressive Damage Accumulation in Composites," Proceedings of International Symposium on Composite Materials and Structures, June 10-13, 1986, pp. 516-521, Beijing, China.

Engblom, J. J. and Ochoa, O. O., "Finite Element Formulation Including Interlaminar Stress Calculations," Computers and Structures, Vol. 23, No. 2, pp. 241-249, 1986.

Engblom, J. J. and Ochoa, O. O., "Through-The-Thickness Stress Predictions for Laminated Plates of Advanced Composite Materials," International Journal for Numerical Methods in Engineering, Vol. 21, pp. 1759-1776, 1985.

Ochoa, O. O., Engblom, J. J. and Tucker, R., "A Study of Effects of Kinematic and Material Characteristics on the Fundamental Frequency Calculations of Composite Plates," Journal of Sound and Vibration, Vol. 101, No. 2, pp. 141-148, 1985.

Engblom, J.J. and Ochoa, O.O., "Through-the-Thickness Stress Predictions for Advanced Composite Material Configurations," 25th Structures, Structural Dynamics and Materials Conference, Part 1, AIAA Paper 84-0859, Palm Springs, California, May 14-16, 1984.

Conference Presentations:

Havelka, J.J. and Engblom, J.J., "An Analysis of the Progression of Damage in Laminated Composites Under Transient Loading," Accepted for Presentation at Pan American Congress of Applied Mechanics, Rio de Janeiro, Brazil, January, 3-6, 1989.

Engblom, J. J. and Parchuri S., "Damage Assessment in Composite Plates," Pressure Vessels and Piping Conference, Pittsburgh, PA, June 19-23, 1988.

Fuehne, J.P. and Engblom, J.J., "A Doubly-Curved, Shell Finite Element Formulation Including Transverse Stress Effects for Composite Shell Structures," 4th Japan-U.S. Conference on Composite Materials, Washington, D.C., June 27-29, 1988.

Fuehne, J. P. and Engblom J. J., "Finite Element Formulation for Composite Shells with Transverse Shear Effects," Accepted for Presentation at XVIIth International Congress of Theoretical and Applied Mechanics, Grenoble, France, August 21-27, 1988.

Engblom, J. J., Fuehne, J. P. and Hamdallah, J. M., "Transverse Stress Calculations for Laminated Composite Shell Structures Using Plate/Shell Finite Element Formulations," Accepted for Presentation at 3rd Technical Conference on Composite Materials, Seattle, Washington, Sept. 26-29, 1988.

Engblom, J. J., "Modelling the Effects of Intraply Cracking in Composite Laminates at the Sublaminar Level," ASME Pressure Vessels and Piping Conference, San Diego, California, June 29-July 2, 1987.

Ochoa, O.O. and Engblom, J.J., "analysis of Progressive Damage Accumulation in Composites," Proceedings of International Symposium on Composite Materials and Structures, June 10-13, 1986, Beijing, China.

Ochoa, O.O., Kozma, F. and Engblom, J.J., "Stability Analysis of Composite Plates," Proceedings of First International Symposium on computational Mechanics, May 24-29, 1986, Tokyo, Japan.

Engblom, J. J., Fox, N. P., and Ochoa, O. O., "Transient Response of Cross-and-Angle-Ply Composite Plates Due to Transverse Loading," International Conference on Computational Mechanics, May 25-29, 1986, Tokyo, Japan.

Engblom, J. J. and Ochoa, O. O., "Inclusion of Damage Mechanisms in Finite Element Formulation of Composite Material Configurations," Symposium on Advances and Trends in Structures and Dynamics, Washington, DC, October 22-25, 1984.

Engblom, J. J. and Ochoa, O. O., "Through-the-Thickness Stress Predictions for Advanced Composite Material Configurations," 25th Structures, Structural Dynamics and Materials Conference. Palm Springs, California, May 14-16, 1988.

Thesis/Reports:

- Kilpatrick, M. D., "The Inclusion of Damage Effects in an Incremental Finite Element Analysis of Composite Plates," TAMU M.S. Thesis, 1984.
- Fox, N., "Transient Response of Composite Plates due to Transverse Loading," TAMU M.S. report, 1984.
- Kozma, F., "A Study of Buckling of Composite Plates," TAMU M.S. Report, 1984.
- Finkel, H., "A New Triangular Finite Element for Fiber Reinforced Composite Plates," TAMU M.S. Thesis, 1985.
- Tucker, R., "Formulation of Efficient Triangular Plate Element for Laminate Analysis," TAMU M.S. Thesis, 1985.
- Handallah, J. M., "Finite Element Plate Formulation Including Transverse Shear Effects for Representing Composite Shell Structures," TAMU M.S. Thesis, 1987.
- Fuehne, J., "A Doubly Curved, Shell Finite Element Formulation Including Transverse Shear Effects for Composite Shell Structures," TAMU M.S. Thesis, 1988.
- Murry, M.L., "Enhanced Finite Element Analysis Using the PATRAN-G Pre- and Post Processor Program," TAMU M.S. Thesis, 1988.
- Havelka, J.J., "An Analysis of the Progression of Damage in Laminated Composites Under Transient Loading," TAMU M.S. Thesis, 1988.

V. TABLES AND FIGURES

Table 1. Material Properties

Elastic Constants

	Uniaxial Tension	Four-Point Bending
E_1 (GPa)	138	190
E_2 (GPa)	10.6	11
E_3 (GPa)	10.6	11
G_{12} (GPa)	6.4	7.2
G_{13} (GPa)	6.4	7.2
G_{23} (GPa)	6.4	7.2
ν_{12}	0.3	.38
ν_{13}	0.3	.38
ν_{23}	0.3	.38

Strengths

σ_{FN} (MPa)	1500 (1500) *	1502 (1502)
σ_{FS} (MPa)	68	67.5
σ_{MN} (MPa)	40 (246)	41 (250)
σ_{MS} (MPa)	68	67.5
σ_{DN} (MPa)	40	41
σ_{DS} (MPa)	68	67.5

* Terms in parenthesis are the compressive strength.

**Table 2. Damage accumulation of laminate
under uniaxial load (static analysis)
[15/90/-15]_s**

	TF	CF	TM	CM	DL
1	117	0	0	0	0
2	0	0	60	0	0
3	117	0	0	0	0
4	117	0	0	0	0
5	0	0	60	0	0
6	117	0	0	0	0

**Table 3. Damage accumulation of laminate
under uniaxial load (dynamic analysis)
[15/90/-15]_s**

	TF	CF	TM	CM	DL
1	97	0	0	0	0
2	0	0	50	0	0
3	97	0	0	0	0
4	97	0	0	0	0
5	0	0	50	0	0
6	97	0	0	0	0

Table 4. Damage Progression of a 24-ply Laminate $[0]_{24}$
with Aspect Ratio $S=8$ Under the Four-Point
Bending Load. $P_{11}/P_6=1.20$

PLY	TF	CF	TM	CM	DL
1	0	0	0	0	0
2	0	0	0	0	0
3	0	0	0	0	0
4	0	0	0	0	0
5	0	0	0	0	0
6	0	0	0	0	0
7	0	0	0	0	11
8	0	0	0	10	10
9	0	0	0	9	8
10	0	0	0	7	6
11	0	0	0	6	6
12	0	0	0	6	6
13	6	0	6	6	6
14	6	0	6	6	6
15	6	0	6	6	6
16	7	0	6	7	7
17	7	0	7	8	8
18	8	0	8	9	9
19	10	0	9	10	10
20	0	0	11	0	0
21	0	0	0	0	0
22	0	0	0	0	0
23	0	0	0	0	0
24	0	0	0	0	0

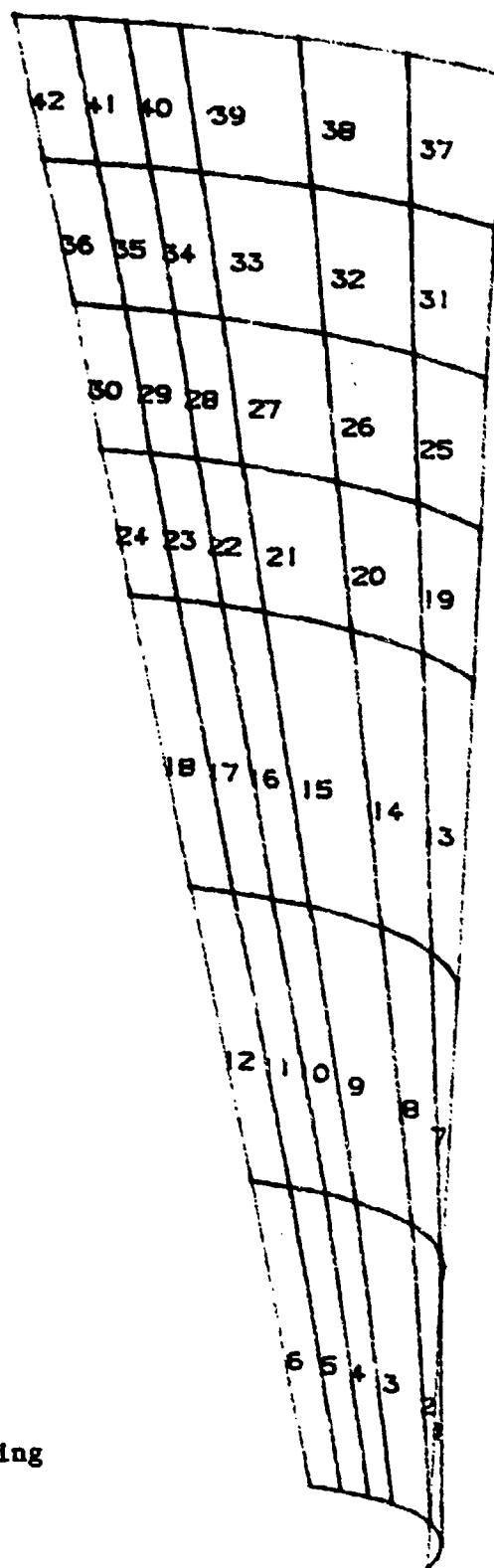


Figure 1. Airfoil Mesh and Element Numbering

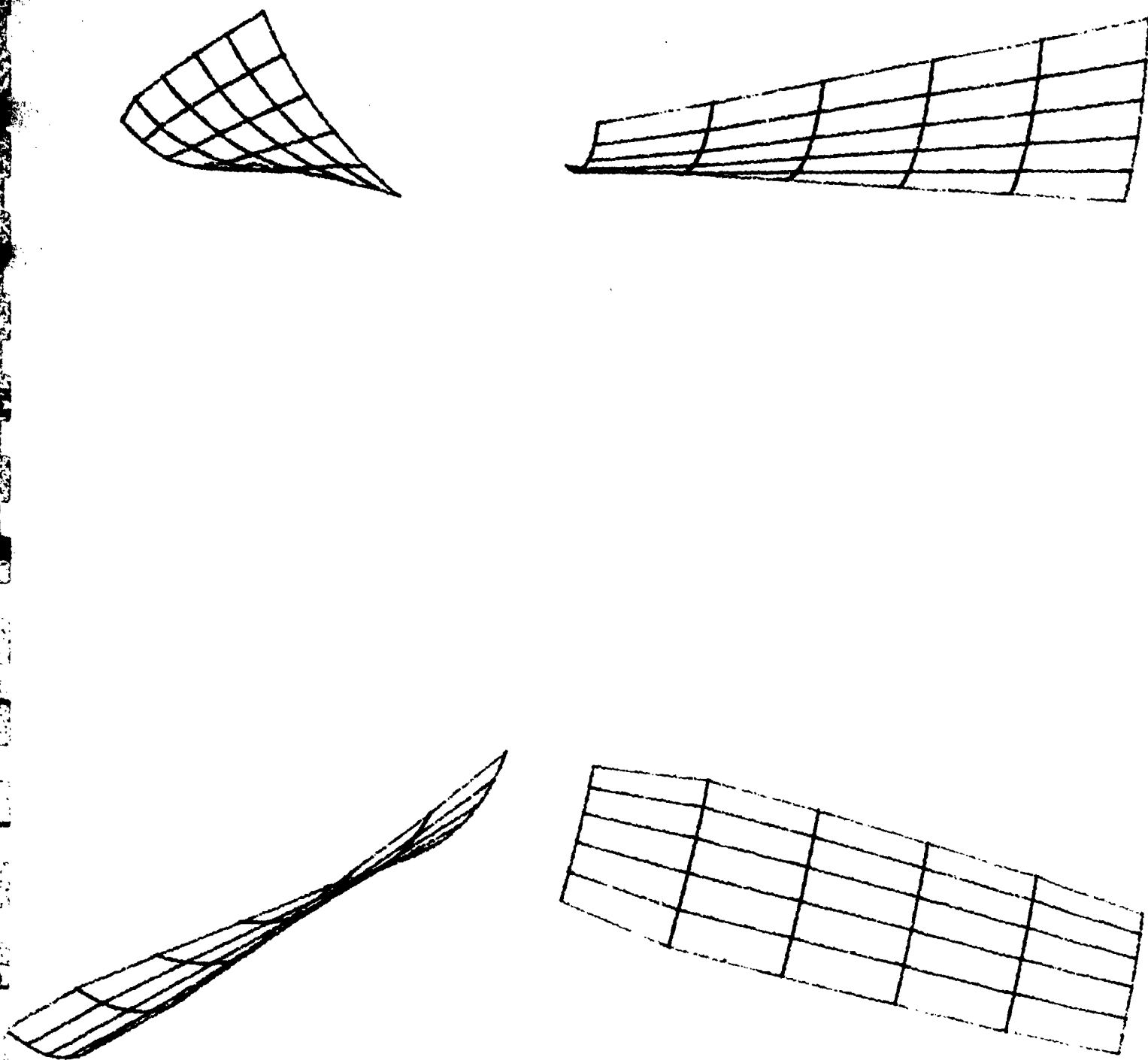


Figure 2. Airfoil Mesh with Multiple Views

TANGENTIAL DISPLACEMENT

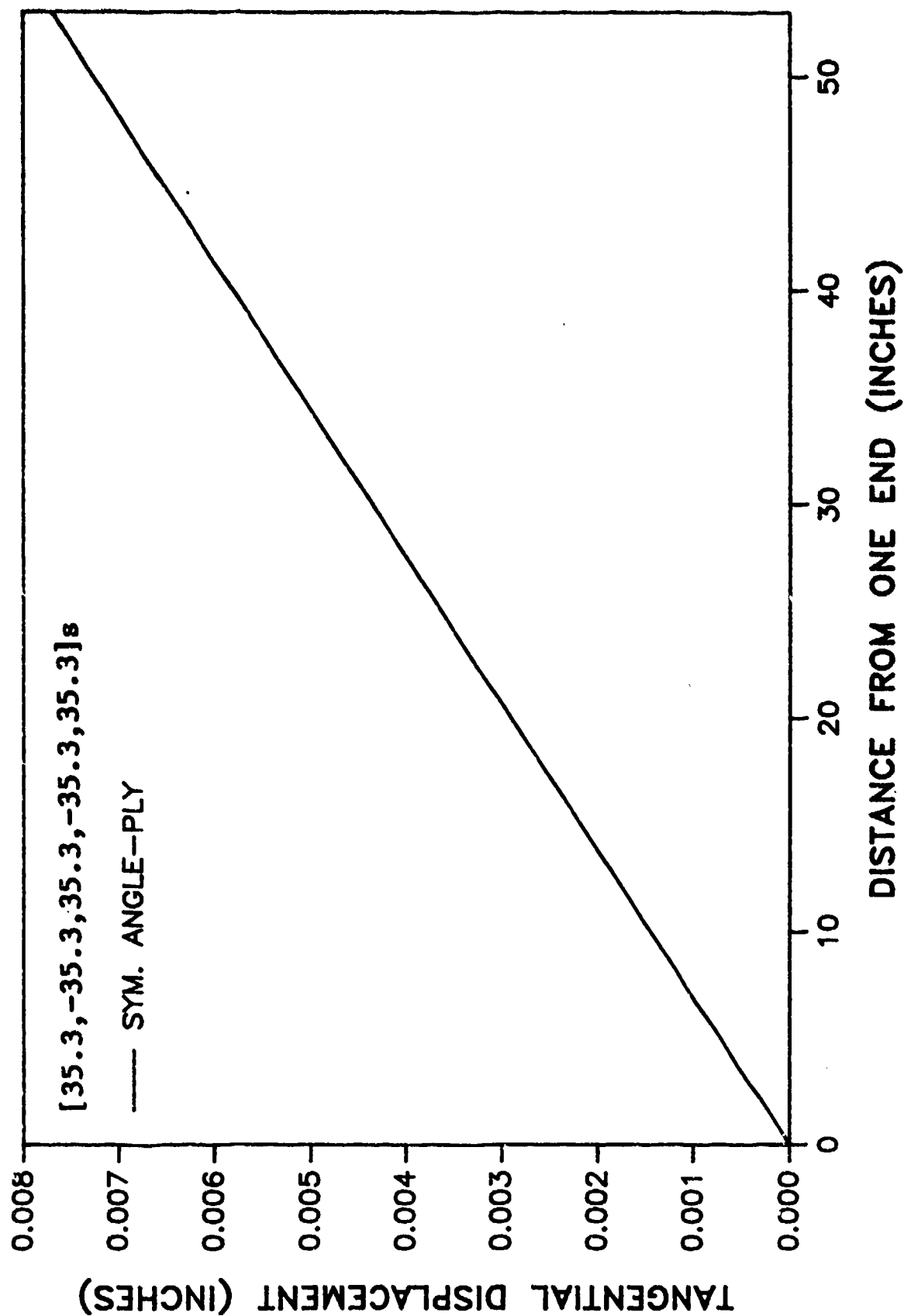


Figure 3

HOOP AND LONGITUDINAL STRESSES

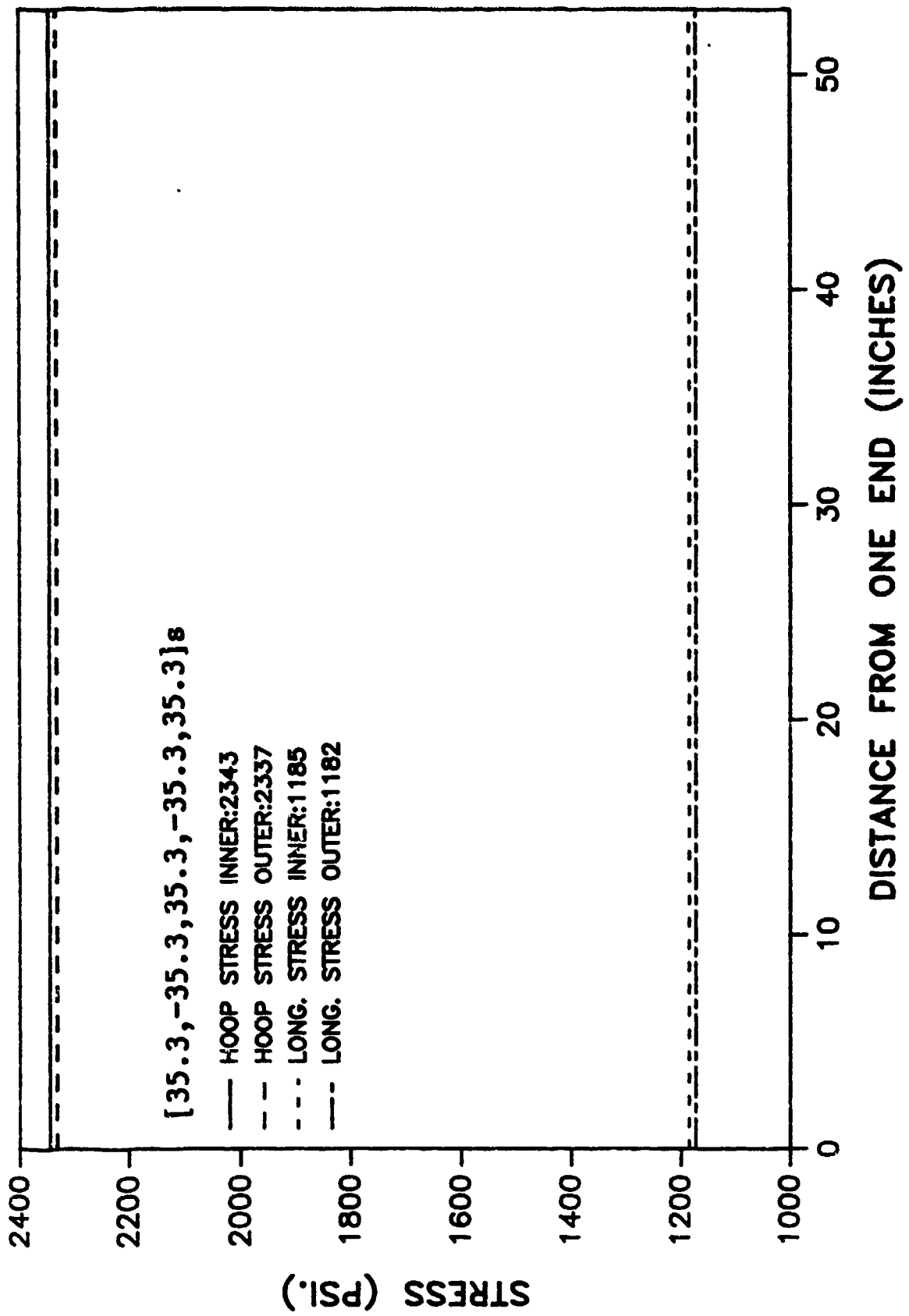


Figure 4

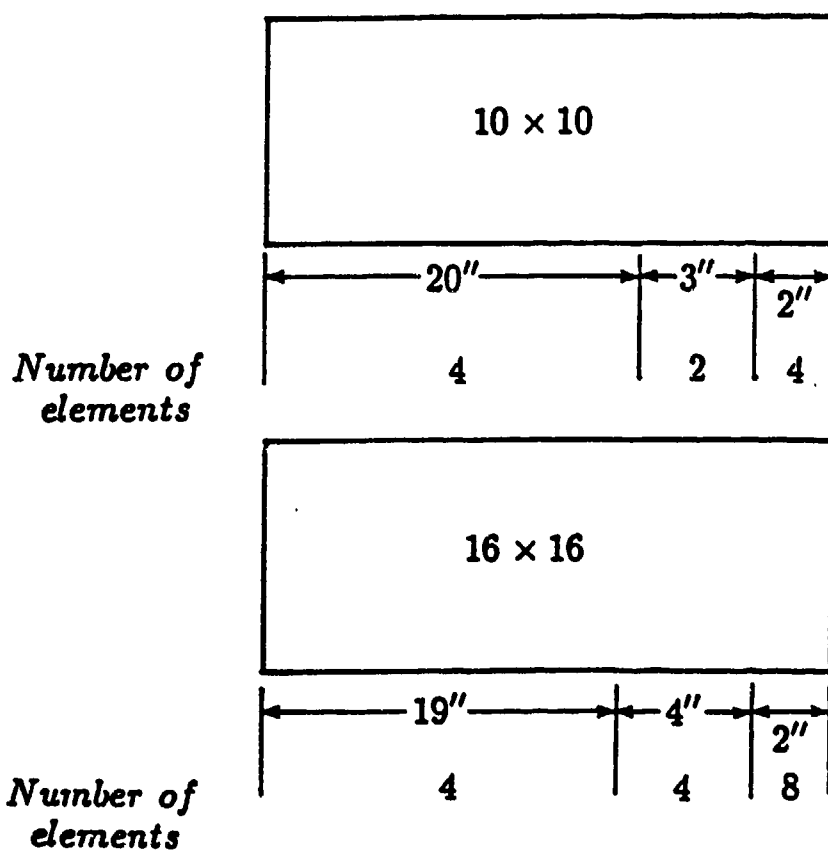
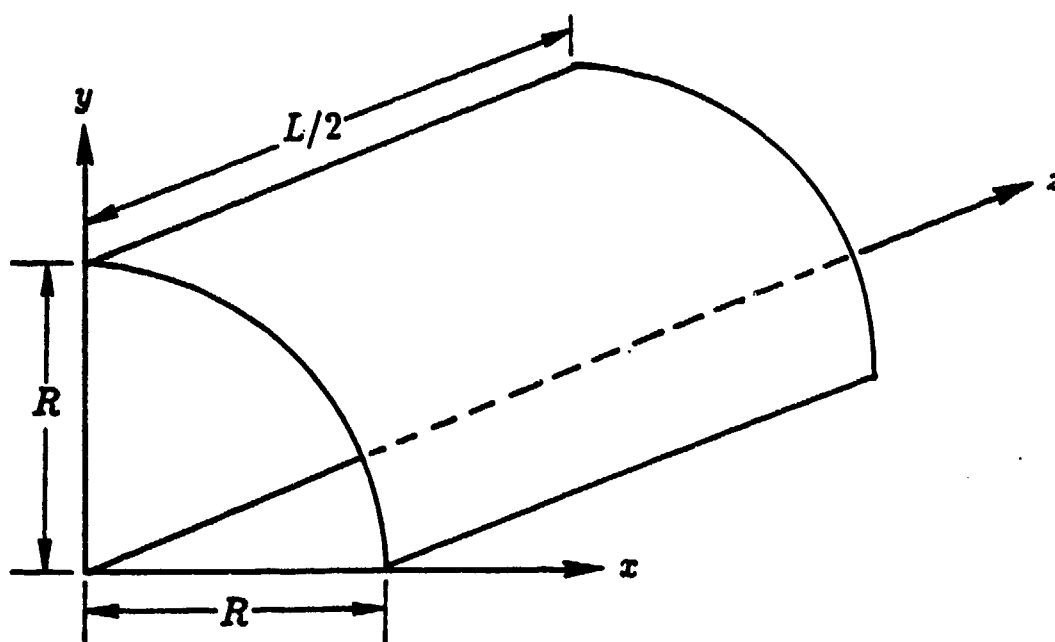


Fig. 5. The reference coordinate system and the two meshes including the dimensions of the elements for the anisotropic, pressurized cylinder.

BORON EPOXY, CROSS-PLY, PRESSURIZED CYLINDER **SIMPLY-SUPPORTED EDGES**

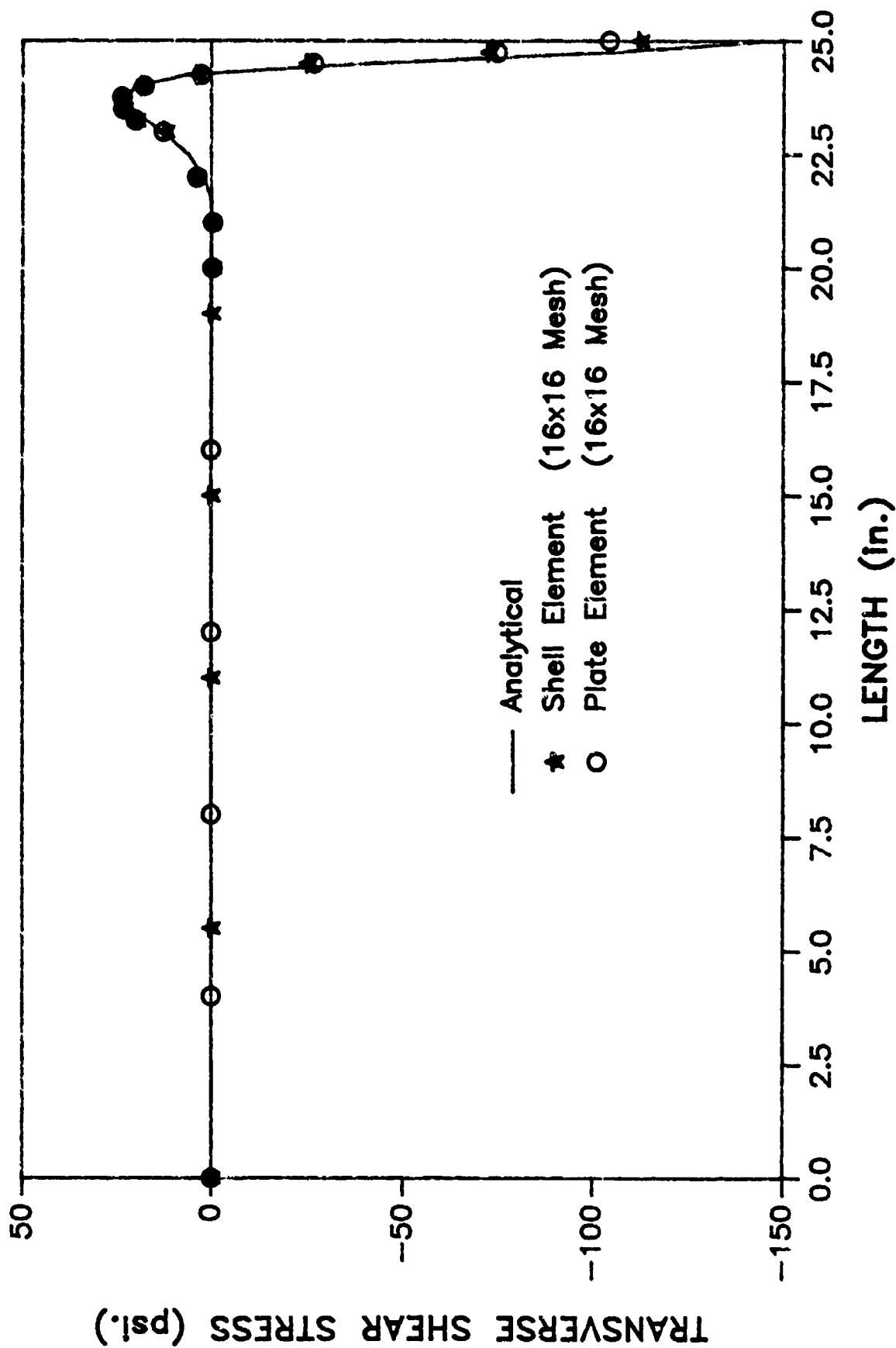


Figure 6. Transverse shear stress at the interface of the 0 and 90 layers for a boron-epoxy cylinder with simply-supported edges.

BORON EPOXY, CROSS-PLY, PRESSURIZED CYLINDER

CLAMPED EDGES

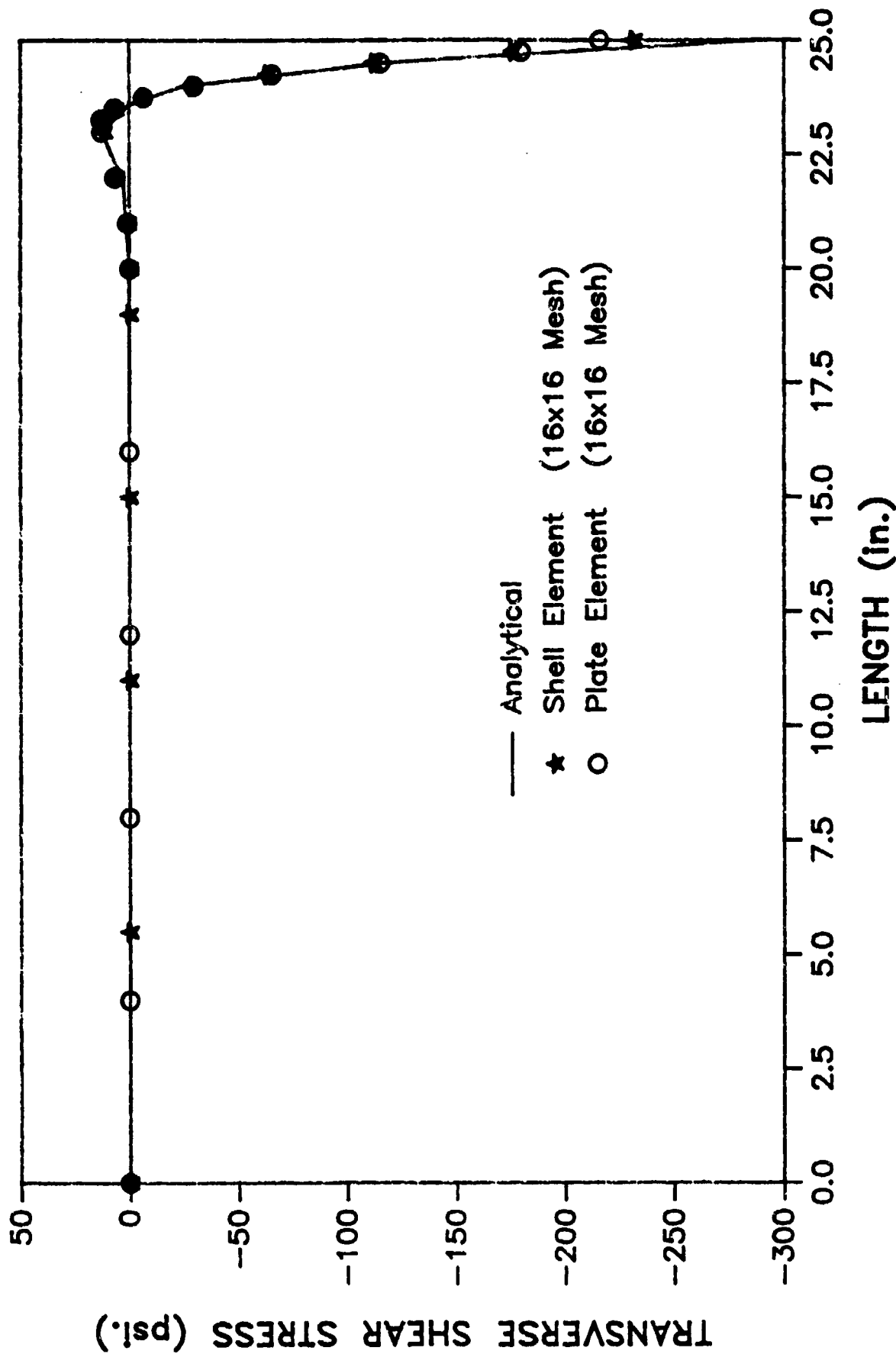


Figure 7. Transverse shear stress at the interface of the 0 and 90 layers for a boron-epoxy cylinder with clamped edges.

GLASS EPOXY, CROSS-PLY, PRESSURIZED CYLINDER SIMPLY-SUPPORTED EDGES

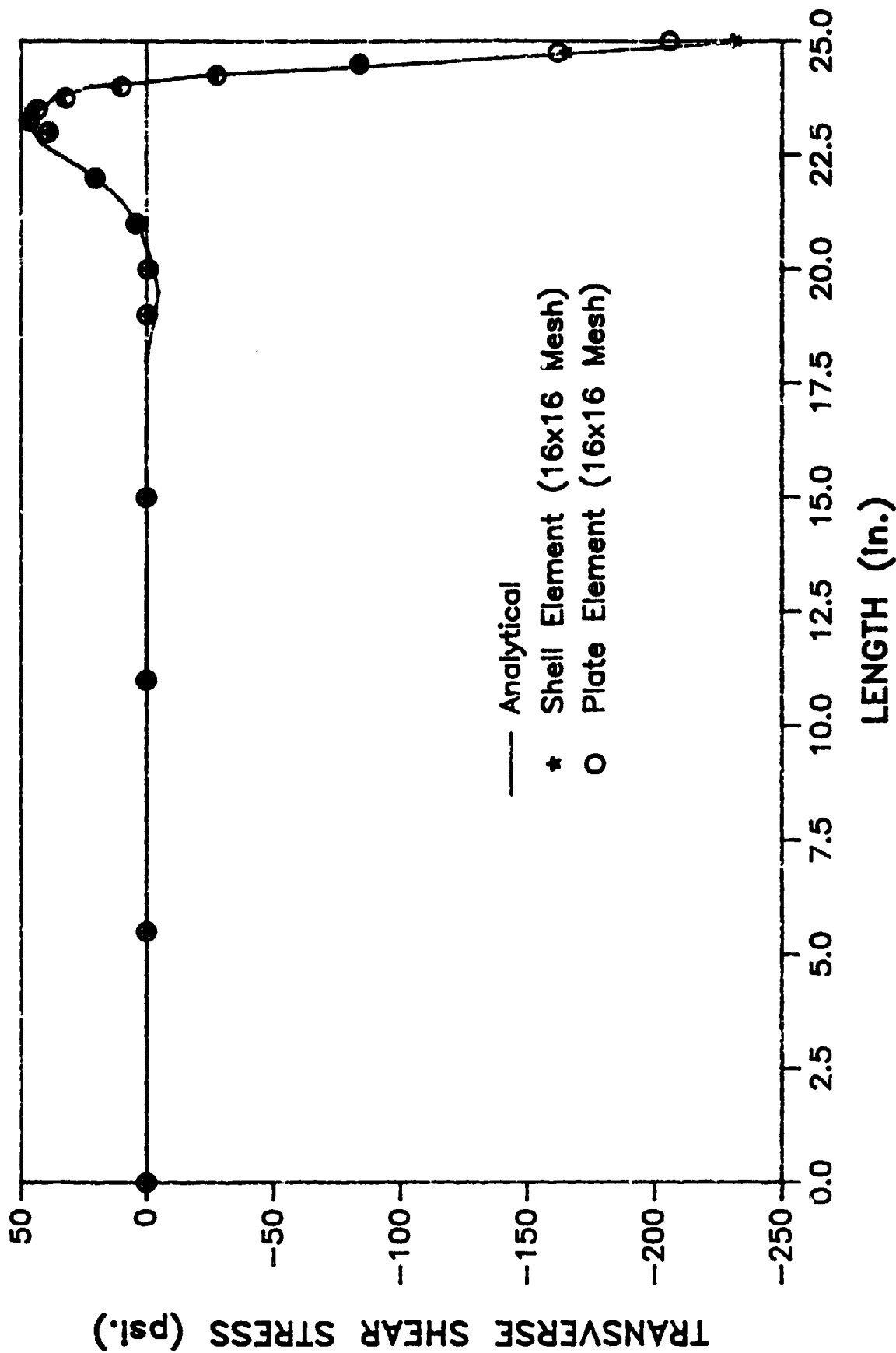


Figure 8. Transverse shear stress at the interface of the 0 and 90 layers for a glass-epoxy cylinder with simply-supported edges.

GLASS EPOXY, CROSS-PLY, PRESSURIZED CYLINDER

CLAMPED EDGES

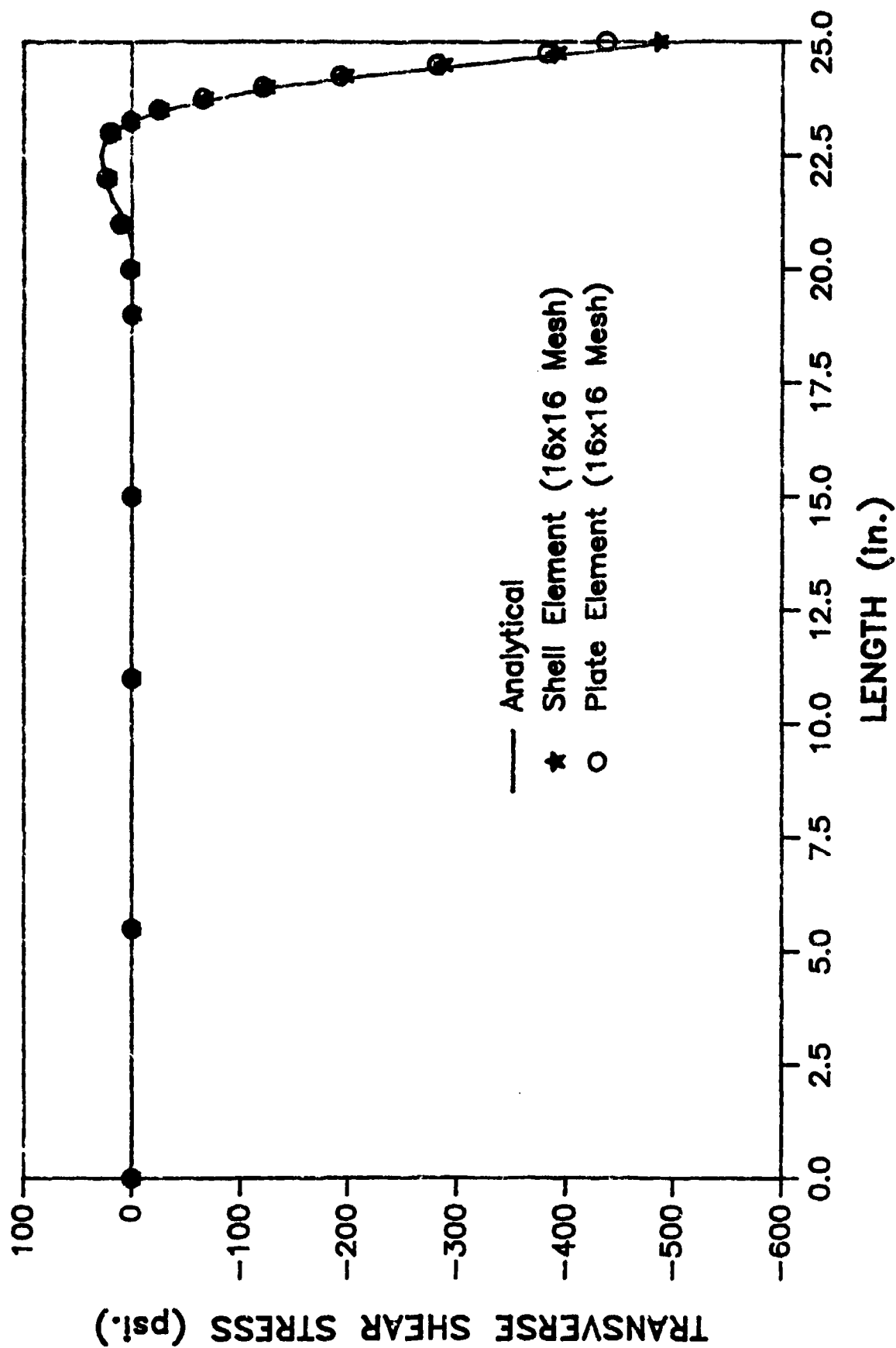


Figure 9. Transverse shear stress at the interface of the 0 and 90 layers for a glass-epoxy cylinder with clamped edges.

GLASS EPOXY, QUASI-ISOTROPIC, PRESSURIZED CYLINDER

SIMPLY-SUPPORTED EDGES

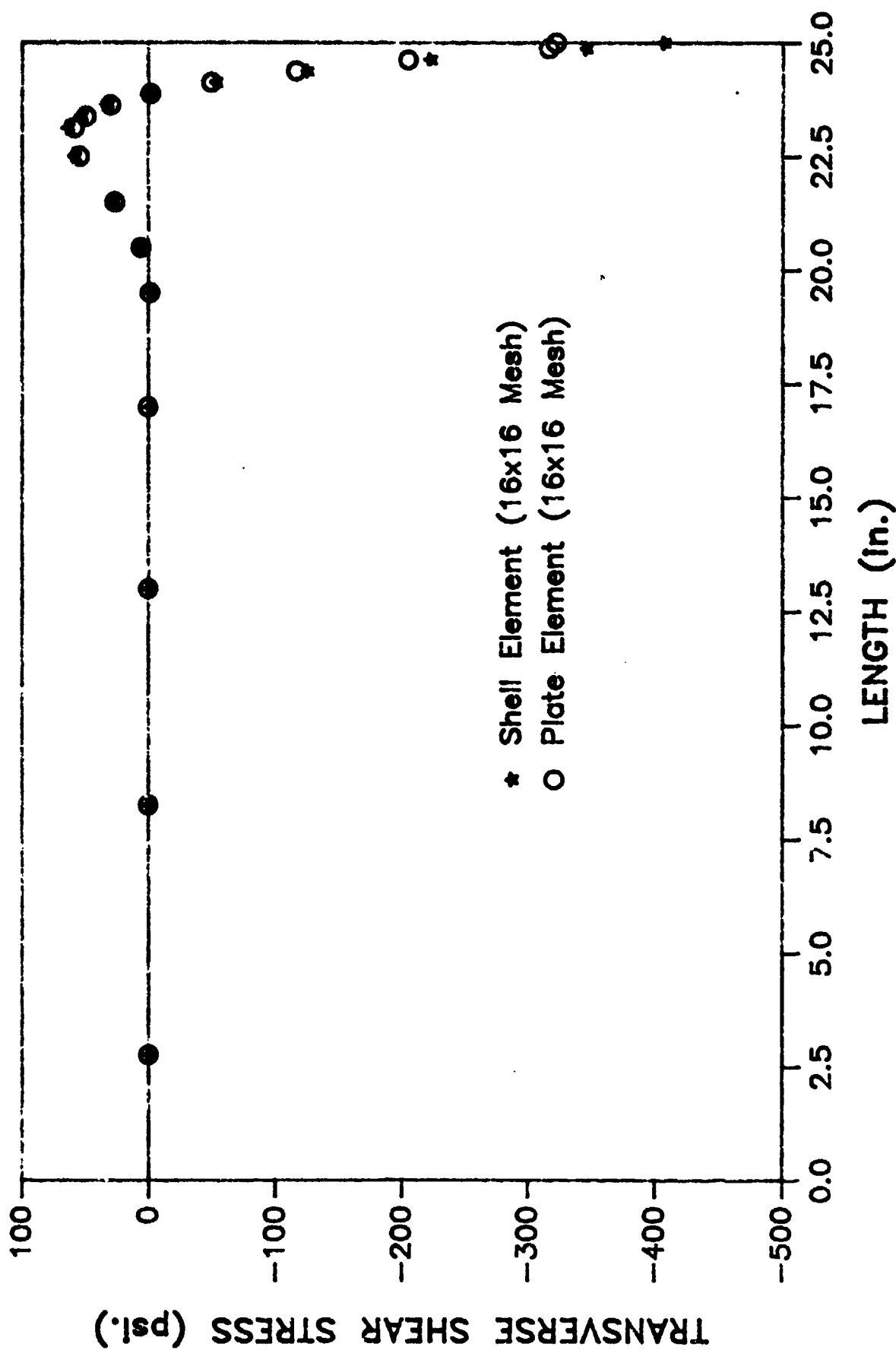


Figure 10. Transverse shear stress at the interface of the -45 and 90 layers for a quasi-isotropic, glass-epoxy cylinder with simply-supported edges.

GLASS EPOXY, QUASI-ISOTROPIC, PRESSURIZED CYLINDER

CLAMPED EDGES

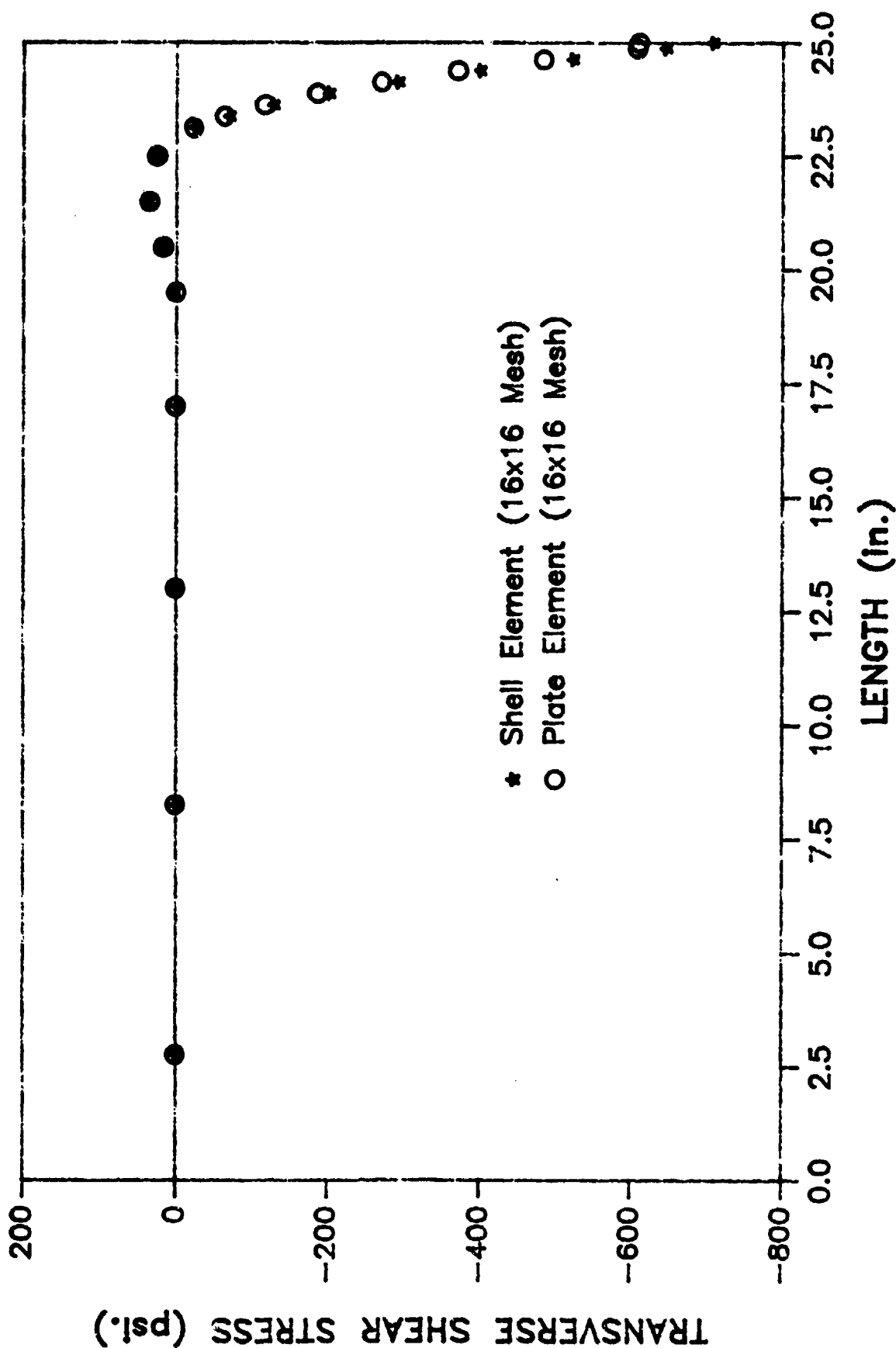
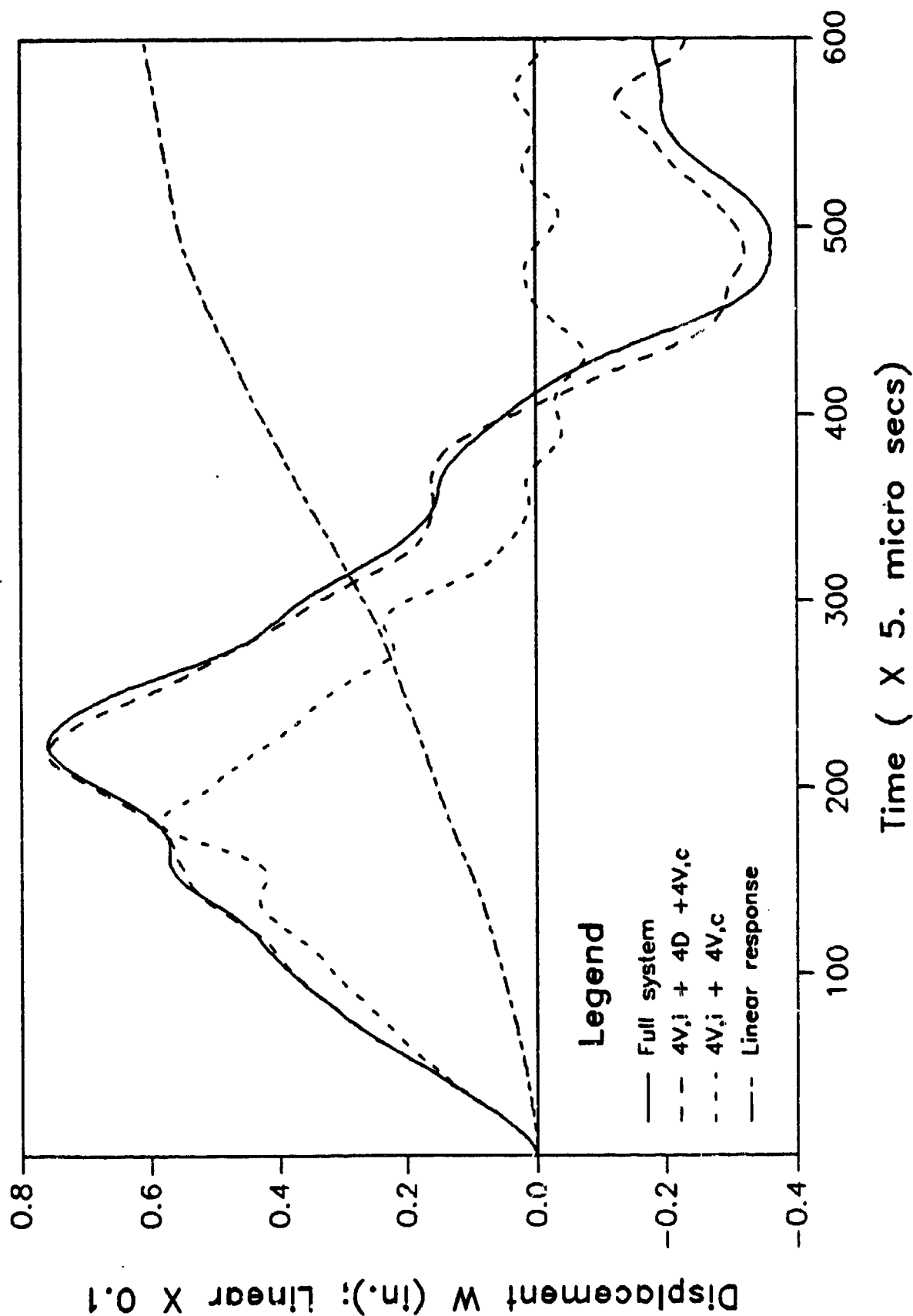


Figure 11. Transverse shear stress at the interface of the -45 and 90 layers for a quasi-isotropic glass-epoxy cylinder with damped edges.

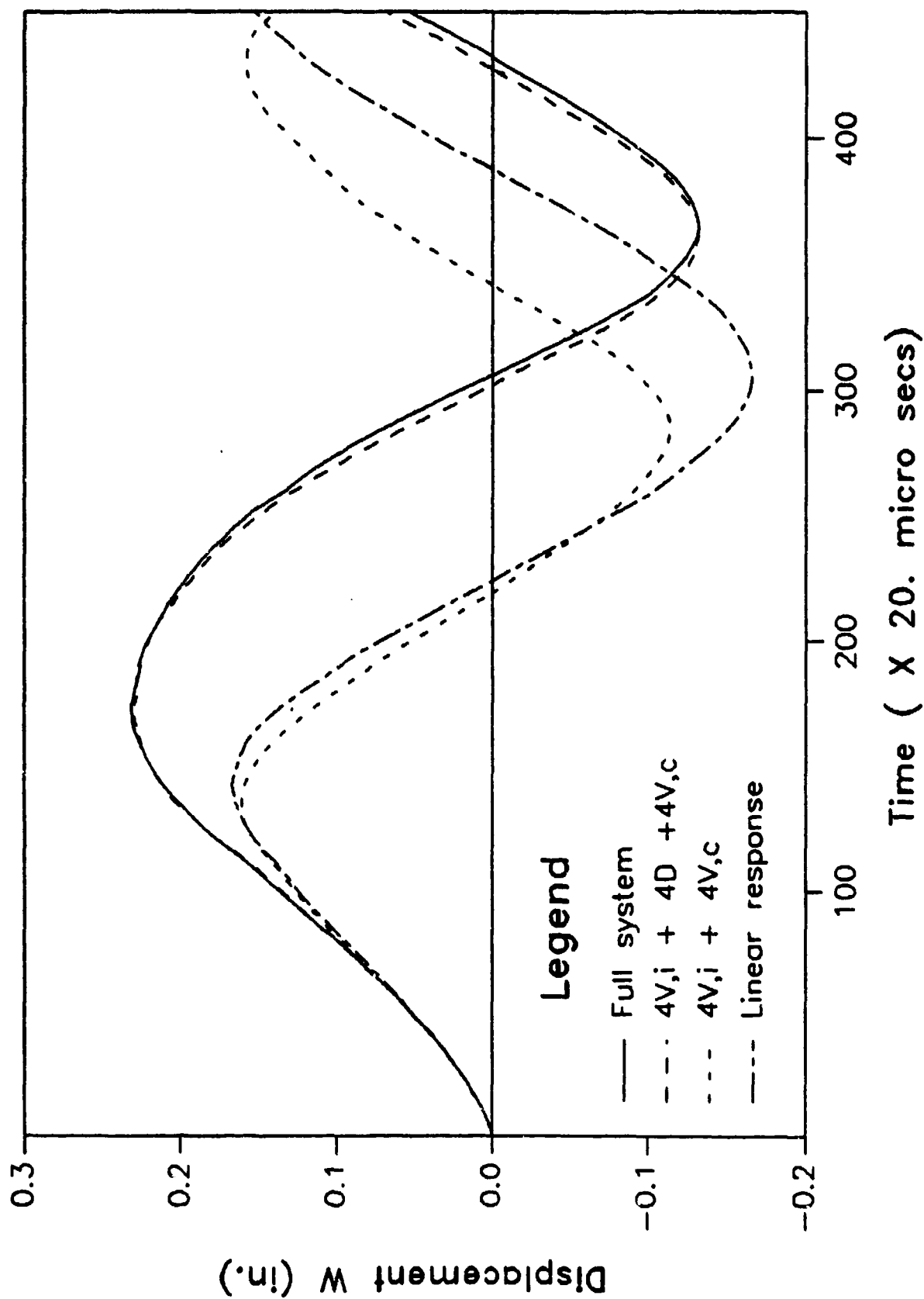
FIGURE 12.

Nonlinear dynamic response of clamped beam



Nonlinear dynamic response of shallow arch

FIGURE 13



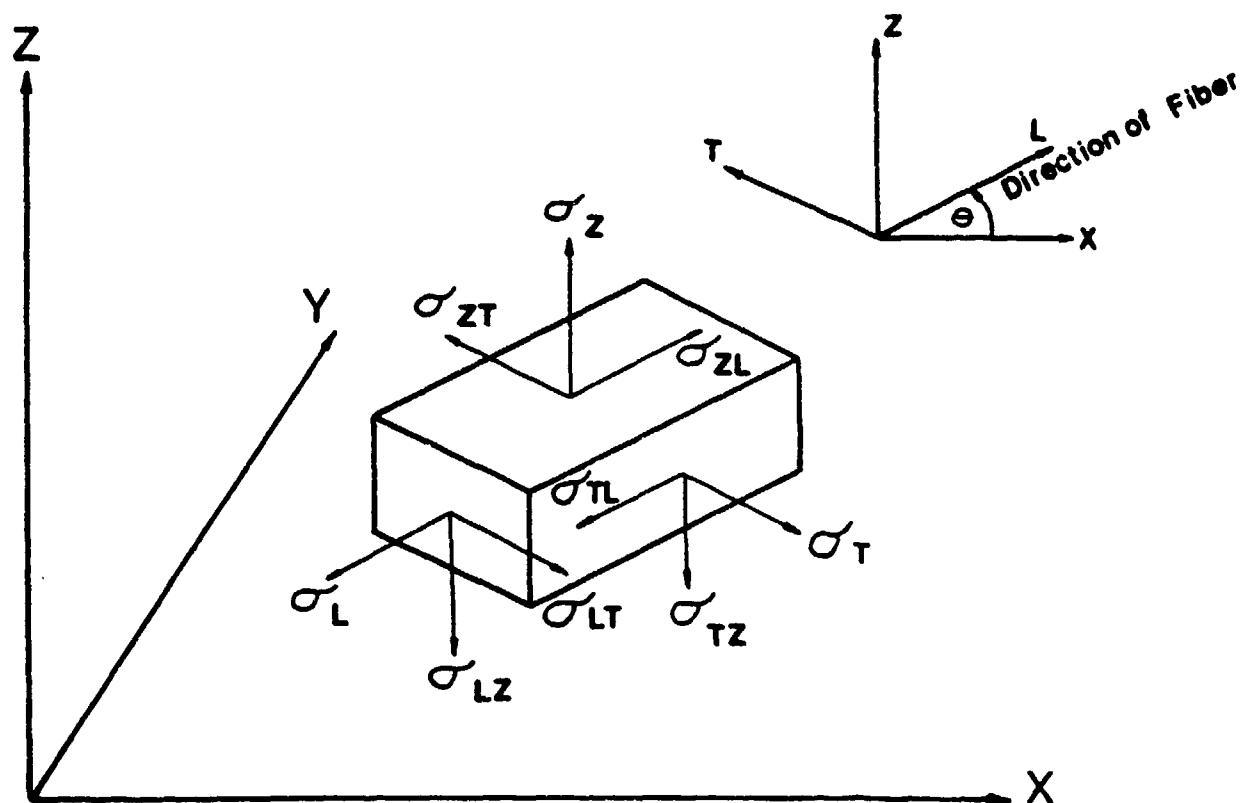


Figure 14. The Stress Components in Natural Coordinates

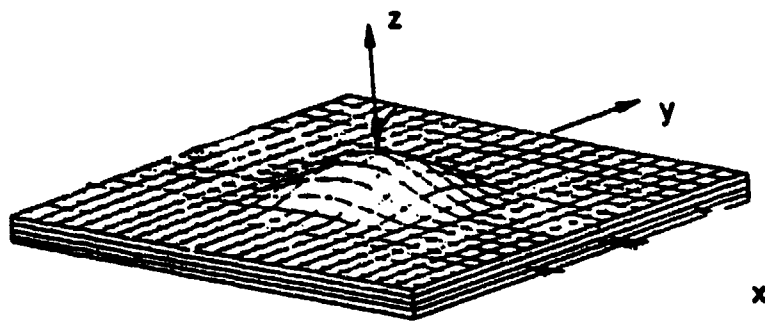
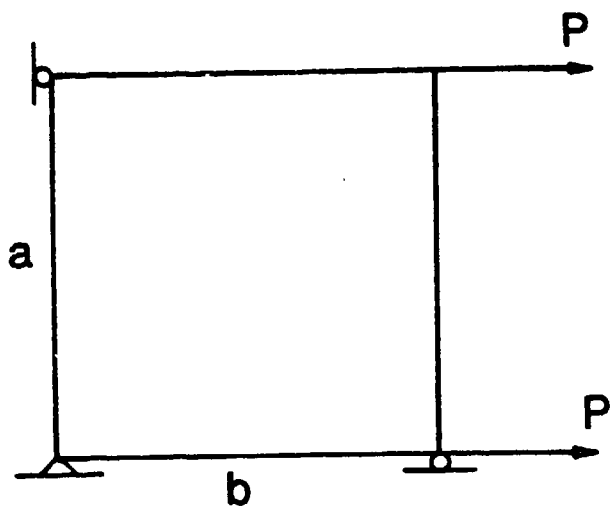


Figure 15. Geometry of sublaminate model



$$a/b = 1$$

$$t/a = 0.00685$$

Figure 16. Uniaxial tension model.

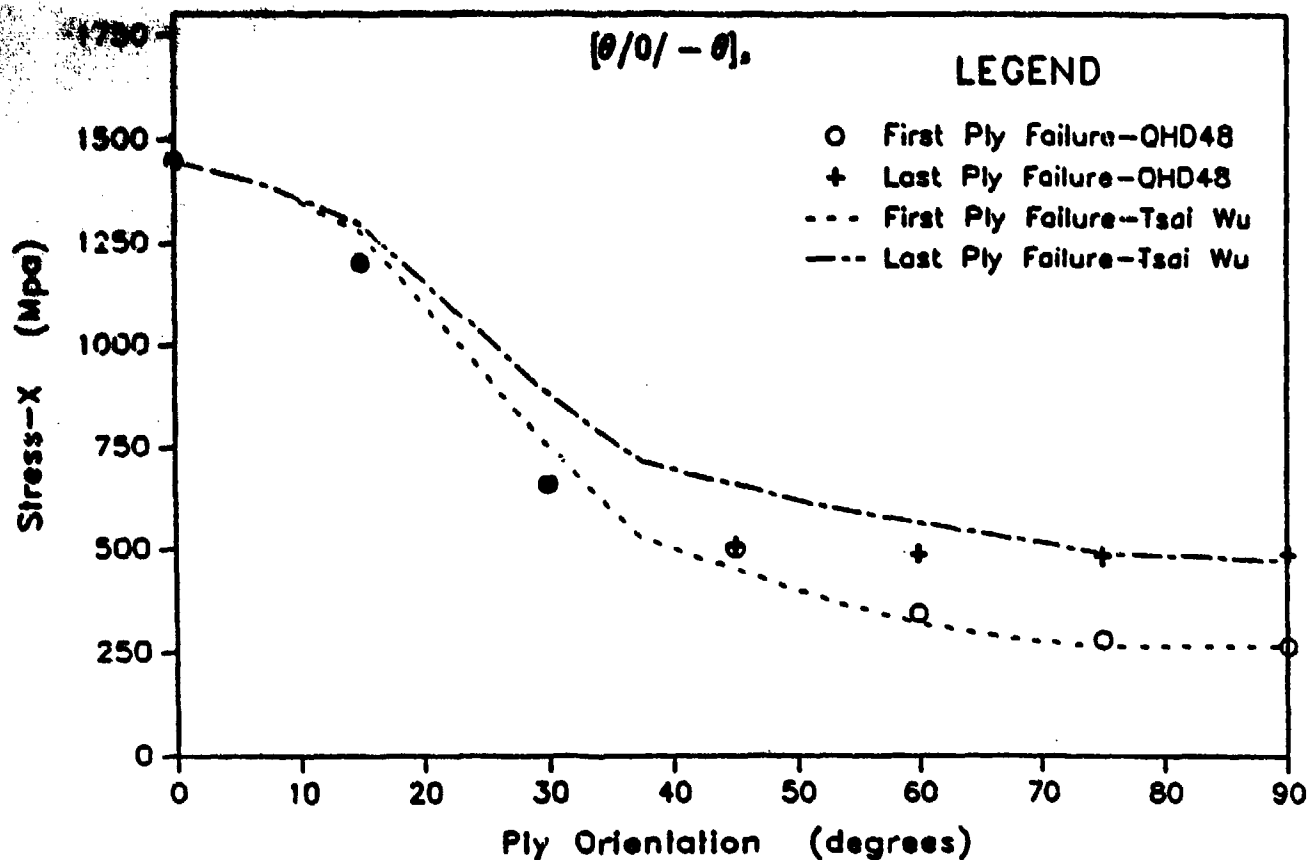


Figure 17. Calculation of first and last ply failure for a $[\theta/0/-\theta]_s$ laminate-nonlinear static analysis

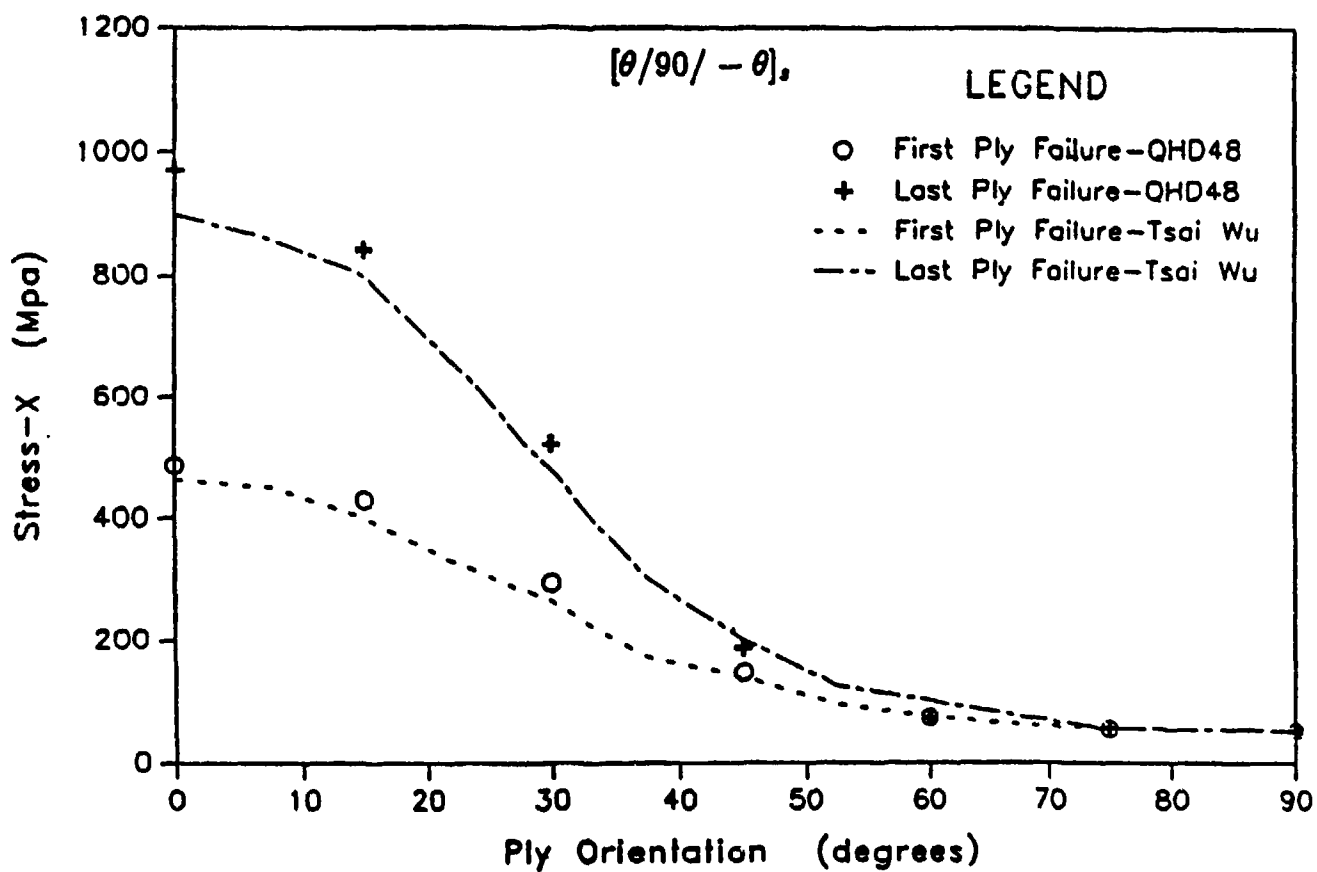


Figure 18. Calculation of first and last ply failure for a $[\theta/90/-\theta]_s$ laminate-nonlinear static analysis

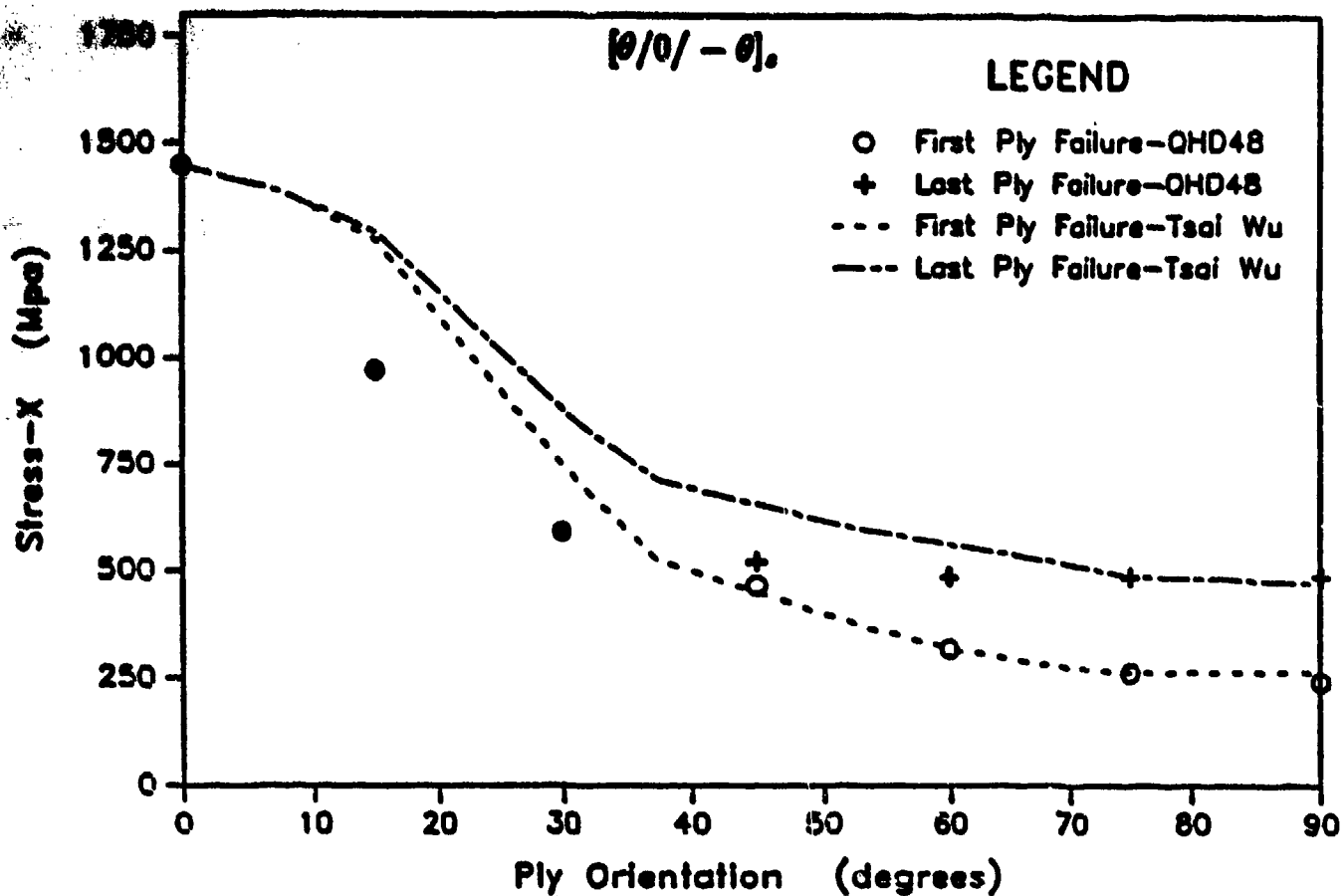


Figure 19. Calculation of first and last ply failure for a critically damped $[\theta/0/-\theta]_s$ laminate-nonlinear dynamic analysis

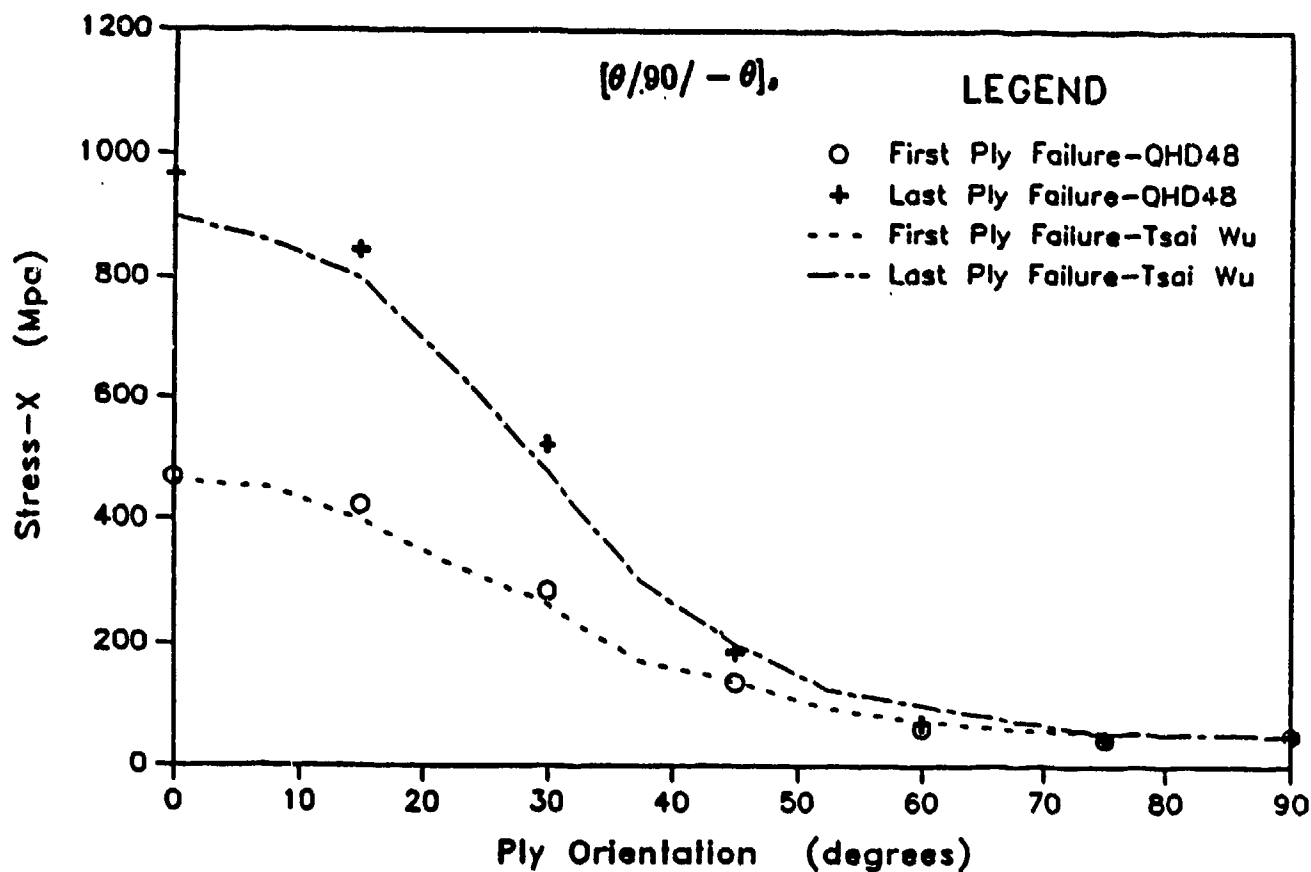


Figure 20. Calculation of first and last ply failure for a critically damped $[\theta/90/-\theta]_s$ laminate-nonlinear dynamic analysis

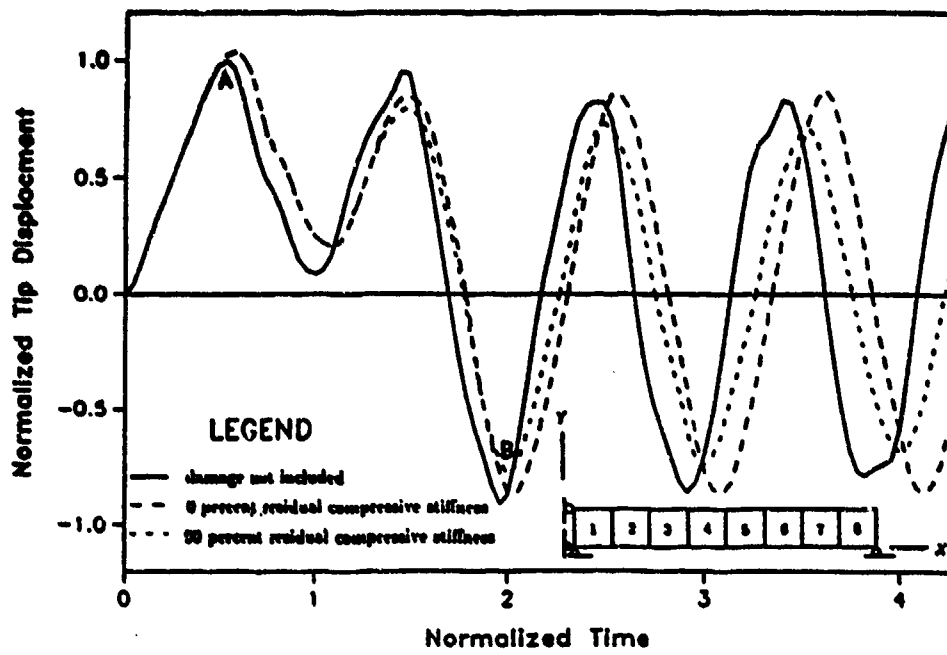


Figure 21 Effects of damage on the transient response of a $[60/0/-60]_s$ composite bar subjected to a rectangular pulse load

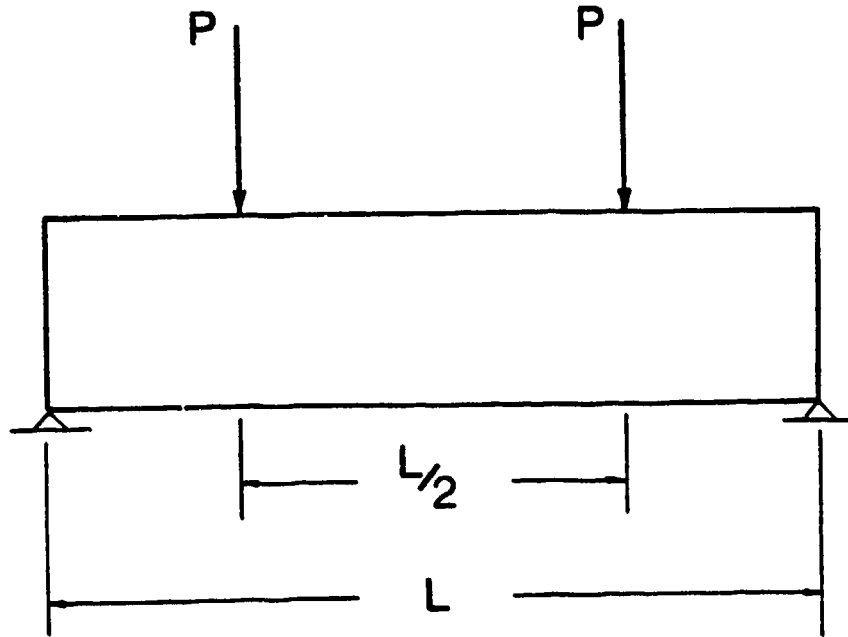


Figure 22. Four-Point Bending Model

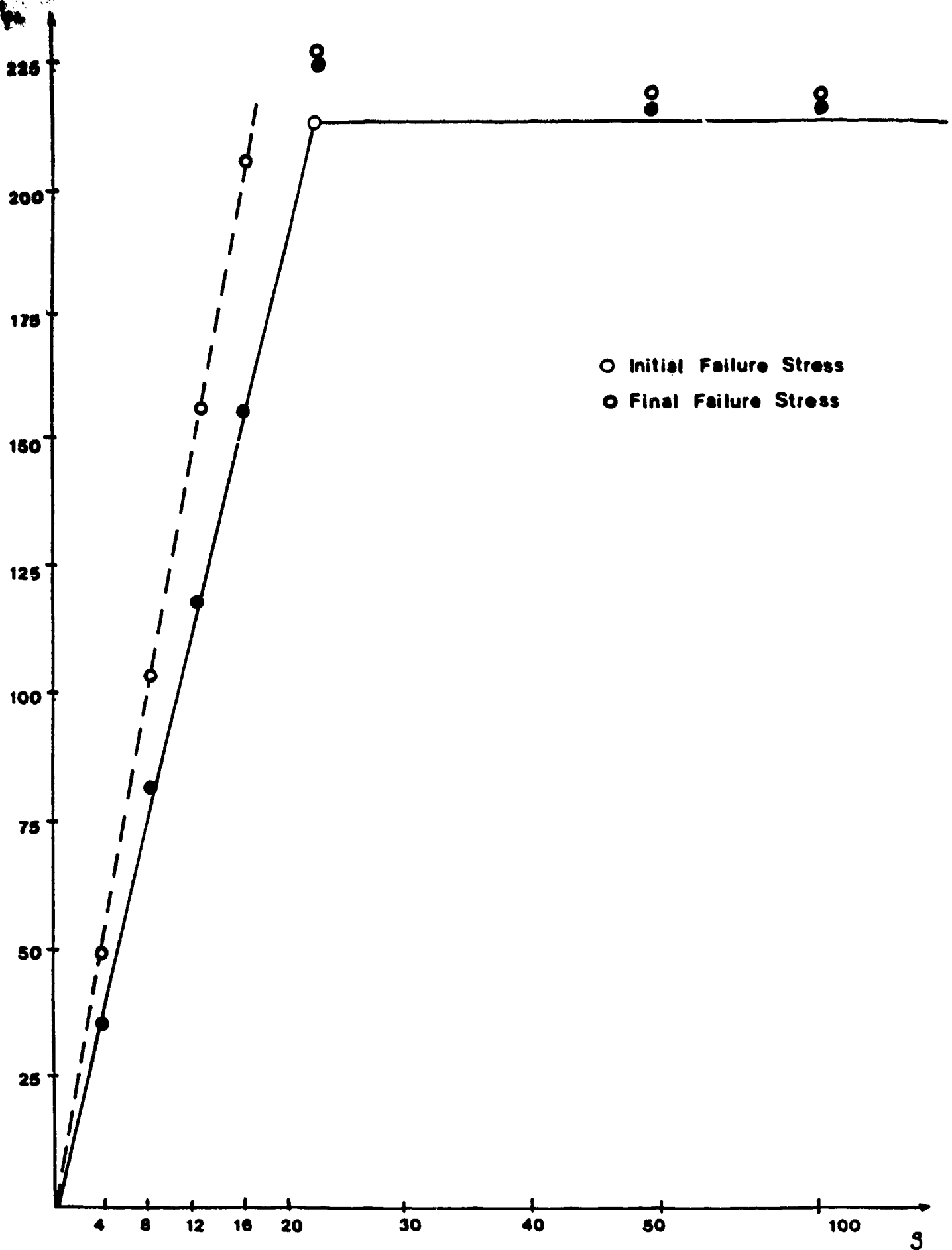


Figure 23. Interaction Curve for Four-Point Bending Load.

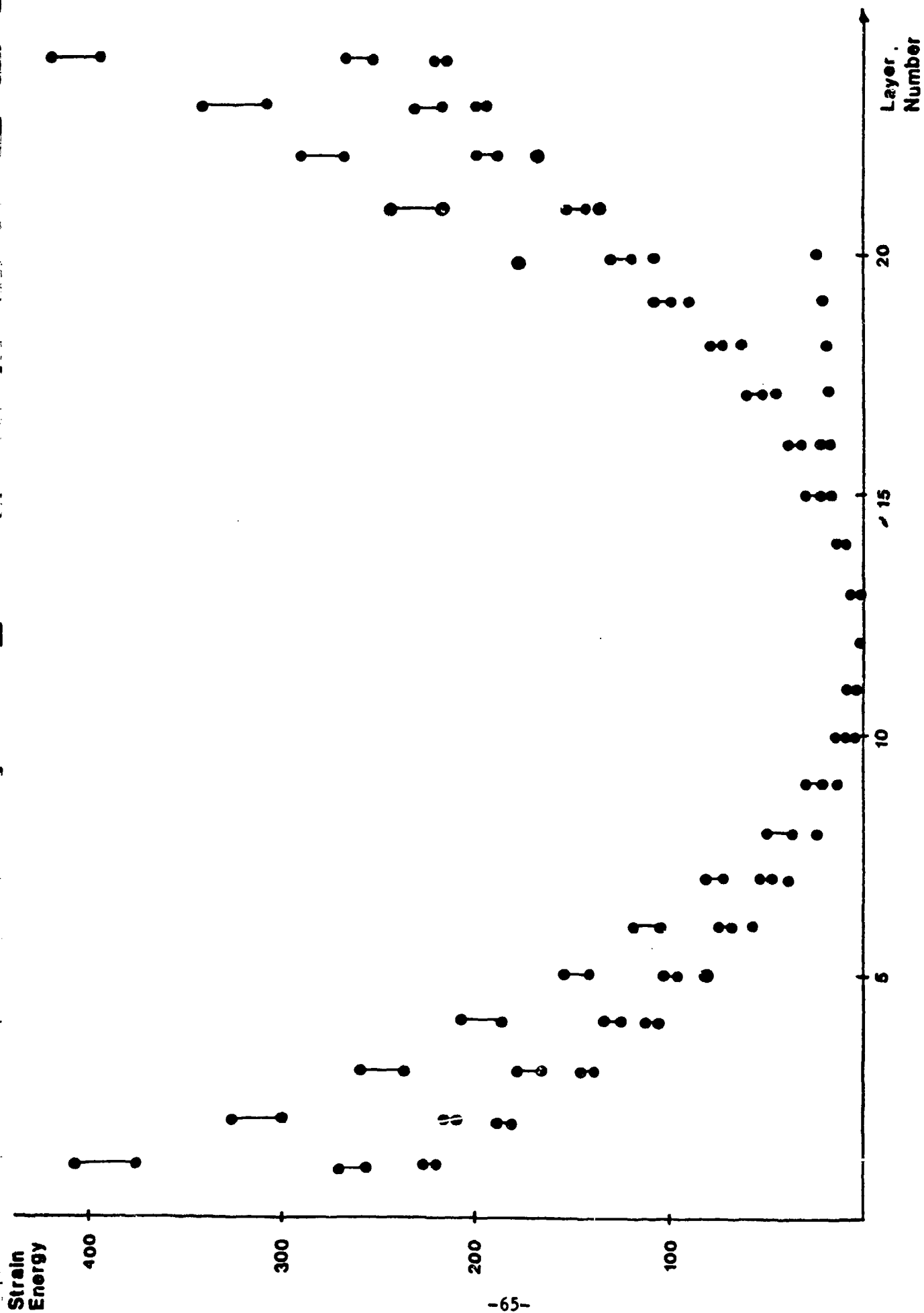


Figure 24. Failure Progression of Four Point Bend Test
aspect ratio = 16

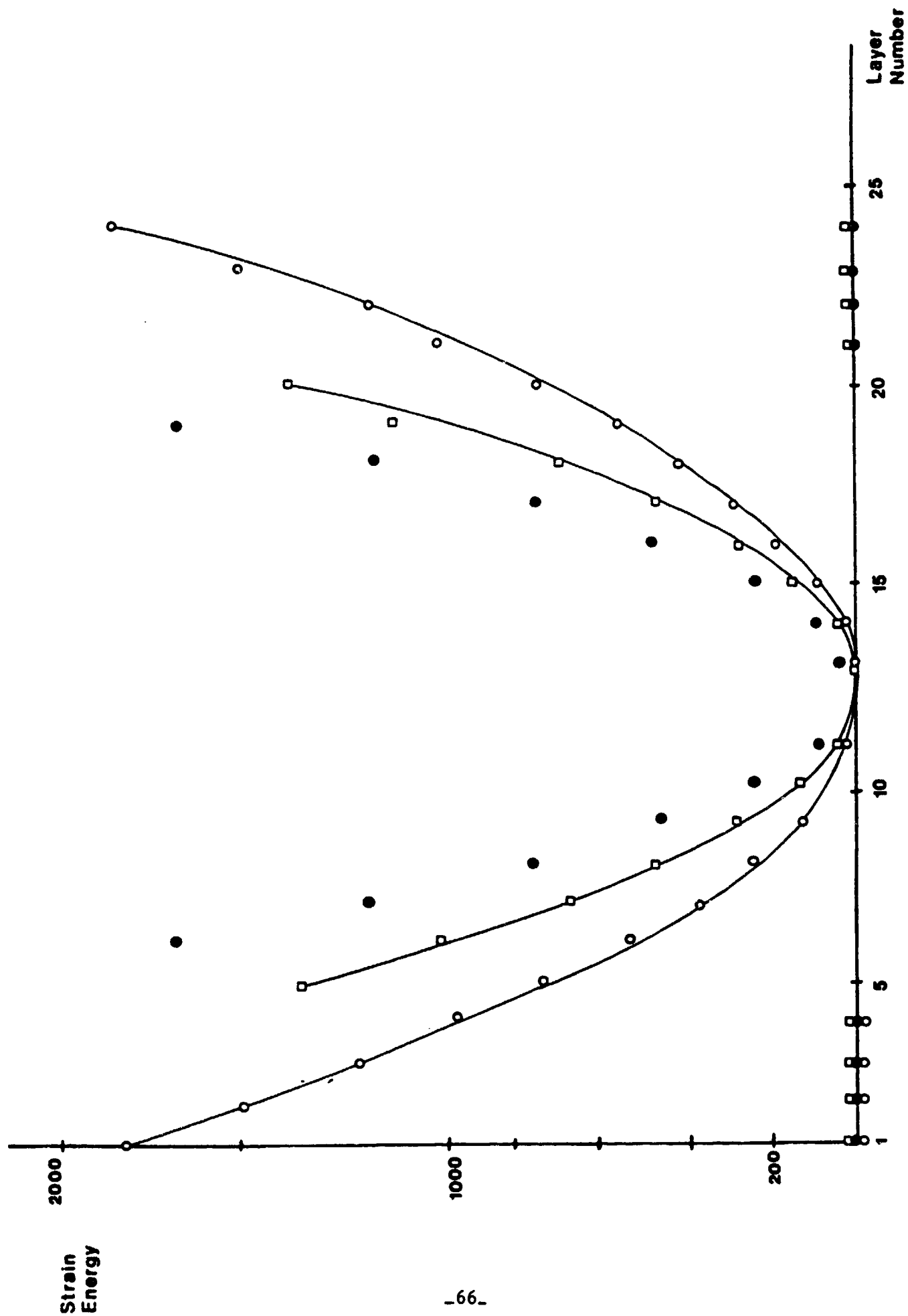


Figure 26. Failure Progression of Four Point Bend Test.

(Percent ratio - 100)

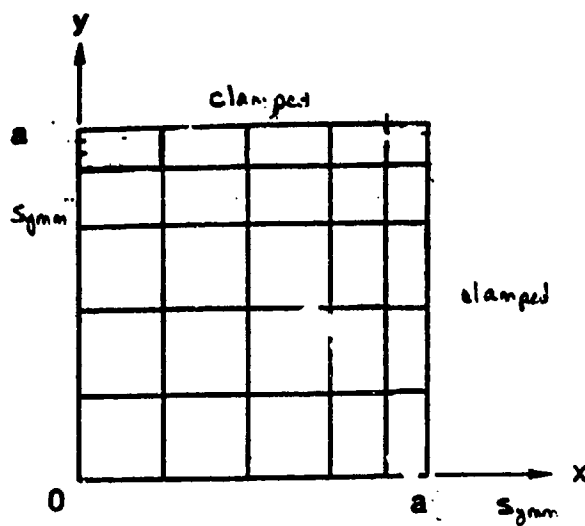


FIGURE 27. Model of Debonded Sublaminate Region

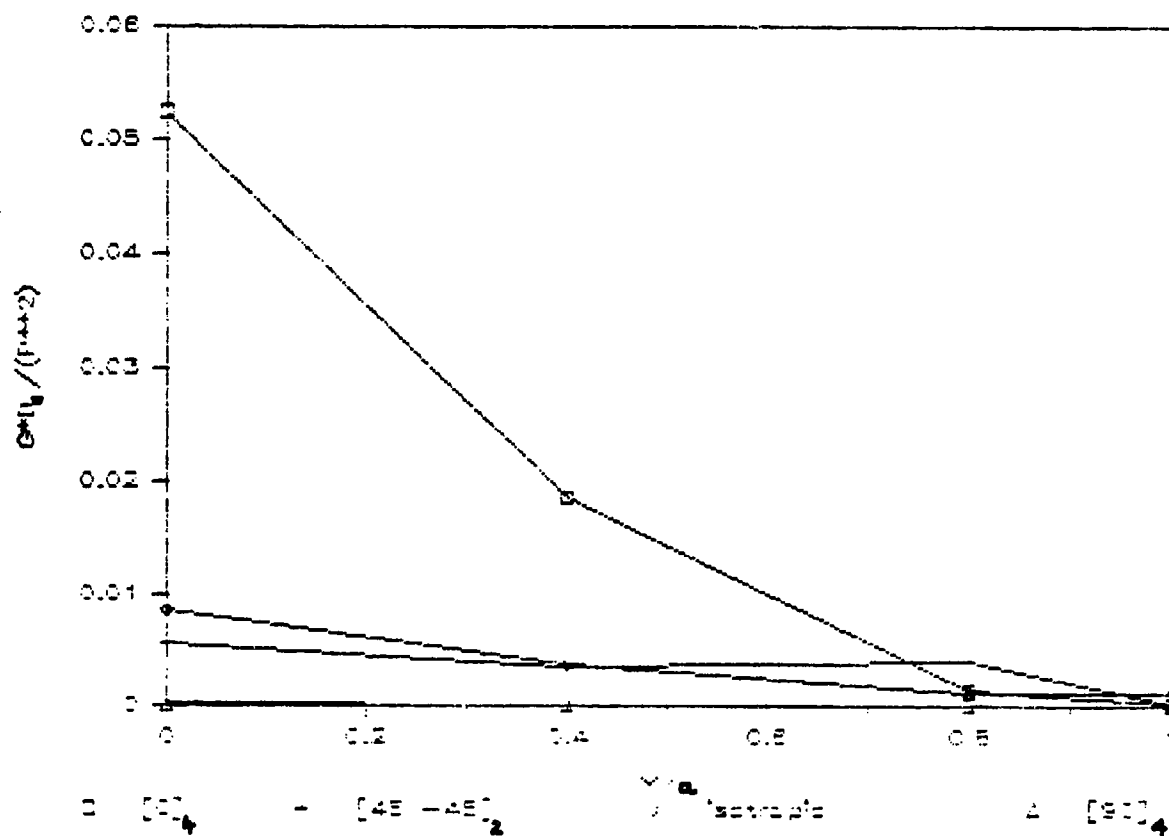


FIGURE 28. G Distribution for Sublaminate Buckling

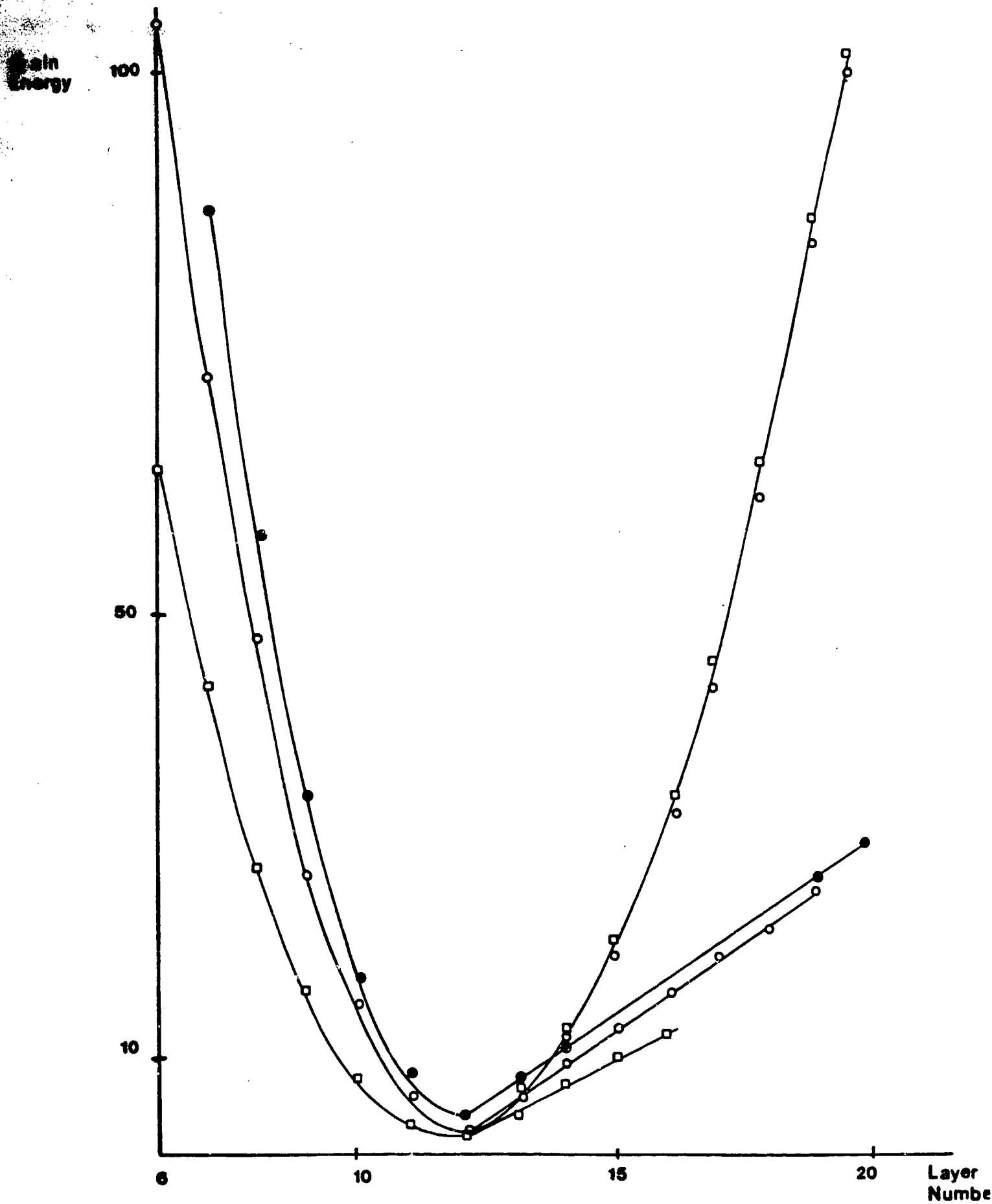


Figure 25 Failure Progression of Four Point Bend Test
(aspect ratio = 16)